Received: 27 October 2022 | Revised: 9 February 2023 | Accepted: 28 April 2023

DOI: 10.1002/cac2.12429

ORIGINAL ARTICLE

CANCER COMMUNICATIONS Open Access

Single-cell atlas reveals a distinct immune profile fostered by T cell-B cell crosstalk in triple negative breast cancer

Shuning Ding[1] | **Niu Qiao**[2] | **Qingchen Zhu**[3] | **Yiwei Tong**[1] | **Shengyue Wang**[2] | **Xiaosong Chen**[1] | **Qiang Tian**[2] | **Yichuan Xiao**[3] | **Kunwei Shen**[1]

[1]Department of General Surgery, Comprehensive Breast Health Center, Ruijin Hospital, Shanghai Jiao Tong University School of Medicine, Shanghai, P. R. China

[2]Shanghai Institute of Hematology, State Key Laboratory of Medical Genomics, National Research Center for Translational Medicine at Shanghai, Ruijin Hospital Affiliated to Shanghai Jiao Tong University School of Medicine, Shanghai, P. R. China

[3]Chinese Academy of Sciences Key Laboratory of Tissue Microenvironment and Tumor, Shanghai Institute of Nutrition and Health, Chinese Academy of Sciences, University of Chinese Academy of Sciences, Shanghai, P. R. China

Correspondence
Xiaosong Chen, Department of General Surgery, Comprehensive Breast Health Center, Ruijin Hospital, Shanghai Jiao Tong University School of Medicine, Shanghai 200025, P. R. China.
Email: chenxiaosong0156@hotmail.com

Qiang Tian, Shanghai Institute of Hematology, State Key Laboratory of Medical Genomics, National Research Center for Translational Medicine at Shanghai, Ruijin Hospital Affiliated to Shanghai Jiao Tong University School of Medicine, Shanghai 200025, P. R. China.
Email: tq12221@rjh.com.cn

Abstract

Background: Characterizing the unique immune microenvironment of each tumor is of great importance for better predicting prognosis and guiding cancer immunotherapy. However, the unique features of the immune microenvironment of triple negative breast cancer (TNBC) compared with other subtypes of breast cancer remain elusive. Therefore, we aimed to depict and compare the immune landscape among TNBC, human epidermal growth factor receptor 2-positive ($HER2^+$) breast cancer, and luminal-like breast cancer.

Methods: Single-cell RNA sequencing (scRNA-seq) was performed on $CD45^+$ immune cells isolated from human normal breast tissues and primary breast tumors of various subtypes. By analyzing the scRNA-seq data, immune cell clusters were identified and their proportions as well as transcriptome features were compared among TNBC, human $HER2^+$ breast cancer, and luminal-like breast

LIST OF ABBREVIATIONS: TIME, tumor immune microenvironment; TNBC, triple negative breast cancer; $HER2^+$, human epidermal growth factor receptor 2-positive; HER2, human epidermal growth factor receptor 2; PR, progesterone receptor; ER, estrogen receptor; IHC, immunohistochemistry; FISH, fluorescence in situ hybridization; ICB, immune checkpoint blockade; PD-1, programmed cell death 1; scRNA-seq, single-cell RNA sequencing; TBCS, T cell-B cell crosstalk prognostic signature; UMI, unique molecular identifier; QC, quality control; PCA, principal component analysis; UMAP, Uniform Manifold Approximation and Projection; NK, natural killer; GO, Gene Ontology; METABRIC, Molecular Taxonomy of Breast Cancer International Consortium; HR, hazard ratio; CI, confidential interval; PPI, protein-protein interaction; Treg, regulatory T cell; IFN, interferon; TF, transcription factor; DEG, differentially expressed gene; TBCS, prognostic signature based on T cell-B cell crosstalk; RFS, relapse-free survival; OS, overall survival; DC, dendritic cell; pDC, plasmacytoid dendritic cell; Breg, regulatory B cell; FACS, fluorescence-activated cell sorting; Tfh, Follicular helper T.

Shuning Ding, Niu Qiao, and Qingchen Zhu contributed equally to this work.

Yichuan Xiao, Chinese Academy of Sciences Key Laboratory of Tissue Microenvironment and Tumor, Shanghai Institute of Nutrition and Health, Chinese Academy of Sciences, University of Chinese Academy of Sciences, Shanghai 200031, P. R. China.
Email: ycxiao@sibs.ac.cn

Kunwei Shen, Department of General Surgery, Comprehensive Breast Health Center, Ruijin Hospital, Shanghai Jiao Tong University School of Medicine, Shanghai 200025, P. R. China.
Email: kwshen@medmail.com.cn

Funding information
National Natural Science Foundation of China, Grant/Award Numbers: 82072937, 82072897, 82002773; Shanghai Municipal Education Commission-Gaofeng Clinical Medicine Grant, Grant/Award Number: 20172007; Science and Technology Commission of Shanghai Municipality Shanghai Sailing Program, Grant/Award Number: 21YF1427400

cancer. Pseudotime and cell-cell communication analyses were also conducted to characterize the immune microenvironment.

Results: ScRNA-seq data of 117,958 immune cells were obtained and 31 immune clusters were identified. A unique immunosuppressive microenvironment in TNBC was decoded as compared to that in HER2$^+$ or luminal-like breast cancer, which was characterized by higher proportions of regulatory T cells (Tregs) and exhausted CD8$^+$ T cells and accompanied by more abundant plasma cells. Tregs and exhausted CD8$^+$T cells in TNBC exhibited increased immunosuppression signature and dysfunctional scores. Pseudotime analyses showed that B cells tended to differentiate to plasma cells in TNBC. Cell-cell communication analyses indicated that these unique features are fostered by the diversified T cell-B cell crosstalk in TNBC. Based on the T cell-B cell crosstalk, a prognostic signature was established that could effectively predict the prognosis status for patients with TNBC. Additionally, it was found that TNBC had a higher proportion of cytotoxic natural killer (NK) cells, whereas HER2$^+$ or luminal-like breast cancer lost this feature, suggesting that HER2$^+$ or luminal-like breast cancer, but not TNBC, may benefit from NK-based immunotherapy.

Conclusions: This study identified a distinct immune feature fostered by T cell-B cell crosstalk in TNBC, which provides better prognostic information and effective therapeutic targets for breast cancer.

KEYWORDS
breast cancer, prognostic signature, single-cell RNA sequencing, T cell-B cell crosstalk, triple-negative breast cancer, tumor immune microenvironment

1 | BACKGROUND

Immunotherapy is becoming a promising treatment option in solid tumors [1]. As the antitumor effect of immunotherapy is strongly associated with the tumor immune microenvironment (TIME), dissecting the complex and heterogeneous TIME is fundamental to finding appropriate therapeutic targets and improving the clinical efficacy of immunotherapies. Triple negative breast cancer (TNBC) is the most aggressive tumor with the worst prognosis compared to luminal-like breast cancer and human epidermal growth factor receptor 2-positive (HER2$^+$) breast cancer [2–4]. Fortunately, immune checkpoint blockade (ICB) has shown remarkable therapeutic effects in TNBC, unlike in luminal-like or HER2$^+$ breast cancer [5–7]. For example, adding pembrolizumab, an anti-programmed cell death 1 (PD-1) monoclonal antibody, to neoadjuvant chemotherapy has yielded a satisfactory pathological complete response rate of 64.8% in TNBC [8]. However, there are still patients with TNBC who do not respond well to immunotherapy, and the underlying mechanisms are poorly understood [9]. Meanwhile, robust biomarkers are lacking to help select patients who can benefit from immunotherapy, and additional effective immunotherapies for luminal-like and HER2$^+$ breast cancer also need to be developed [10, 11]. To address the challenges mentioned above, there is an urgent need for a more comprehensive and in-depth understanding of the unique TIME of each type of breast cancer, especially the distinct features of TNBC in comparison with luminal-like and HER2$^+$ breast cancer.

Previous genomic and transcriptomic studies performed on bulk tumor tissues have provided only averaged information on cellular heterogeneity in the context of TIME. Single-cell RNA sequencing (scRNA-seq) enables transcriptomic analyses of individual cells, providing an unprecedented circumstantial description of immune cell diversity in tumors and allowing a deeper understanding of the complexity of the TIME [12–14]. Several scRNA-seq studies have been carried out in breast cancer, either focusing on single cell populations in TNBC, such as tissue-resident memory T cells [15] and B cells [16], describing the general characteristics of immune cells [17], or depicting the comprehensive tumor environment by sequencing total cells isolated from breast tumors [18, 19]. However, scRNA-seq studies focused on comparing the immune

landscape between TNBC and other breast cancer molecular subtypes are limited. The distinct TIME of TNBC has not yet been explicitly reported.

In this study, scRNA-seq analyses were performed on immune cells isolated from normal breast tissues and primary breast tumors with various molecular subtypes with the aim of elucidating the distinct immune landscape of TNBC compared to that of other molecular subtypes. Cell-cell communications were analyzed to explore the potential roles of immune cell interactions in shaping TIME and to construct a T cell-B cell crosstalk prognostic signature (TBCS) for TNBC. Altogether, this study provided a single-cell resolution transcriptomic atlas of infiltration immune cells and their communications in TNBC compared to those in luminal-like and $HER2^+$ breast cancer, which could lead to new insights for predicting the prognosis and guiding effective therapeutics for patients with breast cancer.

2 | MATERIALS AND METHODS

2.1 | Tissue samples

In this study, tissue samples were obtained from patients undergoing surgical resection. Patients meeting the following criteria were eligible: (1) female; (2) pathologically confirmed invasive ductal breast cancer; (3) undergo breast cancer mastectomy in Ruijin Hospital, Shanghai Jiao Tong University School of Medicine. Patients receiving neoadjuvant systemic treatment or having metastasis at diagnosis were excluded. Patients were pathologically diagnosed with breast cancer by core needle biopsy and then underwent mastectomy. Samples were collected from freshly surgical resections and isolated to single-cell suspensions for scRNA-seq or flow cytometry.

Overall, 17 untreated primary breast cancer tissues and four normal mammary tissues from patients diagnosed with breast cancer from April 2020 to April 2021 were subjected to scRNA-seq. Additional 55 tumor samples and 48 normal samples were collected from May 2021 to December 2021 to conduct flow cytometry. Based on the status of the estrogen receptor (ER), progesterone receptor (PR), and HER2 determined by immunohistochemistry or fluorescence in situ hybridization on surgical resction specimens, which were reported by pathologists in our hospital, tumors were divided into three different molecular subtypes: TNBC (ER^- and PR^- and $HER2^-$), $HER2^+$ breast cancer ($HER2^+$), and luminal-like breast cancer (ER^+/PR^+ and $HER2^-$). The immunohistochemistry and The detailed clinicopathological characteristics of each patient are listed in Supplementary Table S1. This study was approved by the Ethics Committee of Ruijin Hospital, Shanghai Jiao Tong University School of Medicine (ID: 2020-332). The tissue samples were obtained with written informed consent from each patient.

2.2 | Sample preparation

Tissue samples obtained from fresh surgical resections were finely cut into small segments and then digested in RPMI1640 medium (Gibco, Grand Island, NY, USA) containing collagenase IV (1 mg/mL, Gibco) and DNase I (20 μg/mL, Roche diagnostics, Indianapolis, IN, USA) for 60 min on a rotor at 37°C. Digested samples were teased through a 70 μm cell strainer and resuspended in red blood cell lysis buffer (Beyotime, Shanghai, China) to remove red blood cells. Afterwards, the cells were stained with antibodies (anti-human CD45-PE, 304008, 1:200, Biolegend, San Diego, CA, USA) for 30 min at 4°C. Living immune cells (4′,6-diamidino-2-phenylindole-negative [$DAPI^-$], $CD45^+$) were then sorted by fluorescence-activated cell sorting (FACS) Aria SORP flow cytometer (BD Biosciences, San Diego, CA, USA) and subjected to scRNA-seq analysis.

2.3 | Flow cytometry

For the validation of results derived from scRNA-seq analyses, an additional 55 tumor samples and 48 normal samples were collected to conduct flow cytometry, including 7 TNBC, 16 $HER2^+$ breast cancer, and 32 luminal-like breast cancer samples. Samples poorly stained were excluded in further analyses. Single-cell suspensions were prepared and incubated with Livedead (APC cy7, 65-0865-18) and the following antibodies: anti-human Interferon (IFN)-γ (Alexa Fluor 488, 53-7319-42, 1:200), and anti-human CD19 (PEcy7, 25-0199-42, 1: 200) from eBioscience (San Diego, CA, USA); anti-Human FOXP3 (Alexa Fluor 647, 560045, 1: 200) from BD Biosciences; and anti-human CD45 (Alexa Fluor 700, 304024, 1: 200), anti-human CD27 (FITC, 124207, 1: 200), anti-human IgD (Brilliant Violet 510, 348219, 1: 200), anti-human CD38 (Brilliant Violet 421, 562444, 1: 200), anti-human CD3 (PE, 317307, 1: 200), anti-human CD4 (Brilliant Violet 421, 344632, 1: 200), anti-human CD8 (Brilliant Violet 510, 344732, 1: 200), anti-human CD25 (FITC, 302603, 1: 200), anti-human CD56 (APC, 318309, 1: 200), and anti-human CD14 (PEcy7, 367112, 1: 200) from Biolegend. Stained cells were analyzed on a Beckman Coulter Gallios machine (Lane Cove, NSW, Australia).

B cells were identified as $CD45^+CD19^+$ cells; plasma cells were identified as $CD45^+CD19^+CD27^+CD38^+$ cells; cytotoxic $CD8^+$ T cells were identified as $CD45^+$

$CD3^+CD8^+$ IFN-γ^+ cells; and regulatory T cells (Tregs) were identified as $CD45^+CD3^+CD4^+CD25^+FOXP3^+$ cells. For analysis of cytotoxic $CD8^+$T cells, cells were stimulated for 3 h at 37°C with a cell activation cocktail (423303, Biolegend), followed by staining with fixation/permeabilization buffer solution (BD Biosciences) according to the manufacturer's protocol. For Treg detection, cells were stained with fixation/permeabilization buffer solution (eBioscience) according to the manufacturer's protocol.

2.4 | Single-cell RNA library preparation, sequencing, and data analysis

2.4.1 | Single-cell RNA library preparation and sequencing

Single-cell RNA libraries were prepared using the 10 × Chromium Single Cell platform using the Chromium Single Cell 3' Library, Gel Bead and Multiplex Kit, and Chip Kit (10× Genomics, Pleasanton, CA, USA). The loaded viable $CD45^+$ cell numbers ranged from 8,000-16,500 with a final viability of >80%, aiming for 2,000-10,000 single cells per channel. Following the generation of single-cell gel bead-in-emulsions, reverse transcription and amplification were performed. Then, amplified cDNAs were purified and sheared. Purified libraries were sequenced on the NovaSeq 6000 platform (Illumina, San Diego, CA, USA) or the BGI MGISEQ-2000 platform (Shenzhen, China) according to the manufacturer's protocol.

2.4.2 | Single-cell RNA-seq data preprocessing and quality control

The Cell Ranger software pipeline (version 6.0.1) provided by 10× Genomics [20] was applied to demultiplex cellular barcodes, map reads to the GRCh38 reference assembly using the STAR aligner and produce the feature-barcode unique molecular identifier (UMI) matrix. The 21 single-cell RNA libraries were sequenced to average 352,830,238 (260,814,757-456,342,938) paired-end reads per cell with 80.0% (65.3%-98.6%) sequencing saturation (Supplementary Table S2). The UMI count matrix was processed using the R package Seurat (version 4.0.4) [21]. As a quality control (QC) step, genes detected in < 3 cells and cells where < 200 genes had nonzero counts were filtered out. To remove likely doublet captures, cells with total UMI counts > 15,000 with < 200 or > 3,500 detected genes were excluded. Following visual inspection of the distribution of cells with mitochondrial genes, low-quality cells where > 20% of the counts belonged to mitochondrial genes were also discarded. Additionally, the DoubletFinder (version 2.0.3) [22] R package was also applied for each library separately to identify potential doublets. The expected doublet rate was set to be 7.5%, and cells predicted to be doublets were filtered. After QC, a total of 130,128 single cells from 21 libraries were retained for downstream analysis. The stepwise QC metrics used for individual samples are listed in Supplementary Table S2. The resulting distribution of gene counts, UMI counts, as well as mitochondrial gene proportion are shown in Supplementary Figure S1A.

2.4.3 | scRNA-seq normalization, batch effect correction, dimensionality reduction, and unsupervised clustering

After QC and filtering, the feature-barcode matrices of each library were processed by the Seurat (version 4.0.4) [21]. R package was used for normalization, highly variable feature identification, scaling, and linear dimensional reduction. Firstly, all 21 libraries were combined by the Seurat merge function. Library size normalization was performed in Seurat on the filtered matrix to obtain the normalized count by NormalizeData. Features that exhibited high cell-cell variation in the dataset were identified by FindVariableFeatures, and a total of 3,000 highly variable features were returned. Features were then centered and scaled by ScaleData, and principal component analysis (PCA) was conducted by RunPCA. Next, to integrate cells into a shared space from different datasets for unsupervised clustering, the harmony algorithm [23] was used for batch effect correction. A PCA matrix with 30 components that used such informative genes was fed into the RunHarmony function implemented in R package harmony (version 1.0). For visualization, the dimensionality of each dataset was further reduced using the Uniform Manifold Approximation and Projection (UMAP) by the Seurat function RunUMAP. For unsupervised clustering, a K-nearest neighbor based on the Euclidean distance in the PCA space was first calculated and a shared nearest neighbor graph was constructed by FindNeighbors. Then, modularity optimization techniques by the Louvain algorithm were applied by FindClusters to identify clusters of cells.

2.4.4 | scRNA-seq cell subset identification and annotation

The first round of clustering (resolution = 0.3) identified four major cell types, including T cells, B cells, natural killer (NK) cells, and myeloid cells. To identify clusters within each major cell type, a second round of clustering on T, B, NK, and myeloid cells was performed separately.

The procedure of the second round of clustering was the same as that of the first round, starting from low-rank harmony output (30 components) on the highly variable genes chosen as described above, with a resolution ranging from 0.1 to 0.9. The clustree (version 0.4.4) [24] R package was used to visualize and evaluate the above clustering results. Meanwhile, single cells expressing two sets of well-studied canonical markers of major cell types were labeled as doublets and excluded from the following analysis. After this step, a total of 12,170 cells were removed from 130,128 cells, and 117,958 cells were retained for final analysis. In total, four major cell types were identified, including $CD4^+$ and $CD8^+$ T cells (*CD3D, CD3E, CD3G, CD40, CD40LG, CD8A, and CD8B*), B cells (*CD79A, CD79B, MS4A1, and CD19*), NK cells (*GNLY, NKG7, TYROBP, and PRF1*), and myeloid cells (*CST3 and LYZ*). These major cell types were further classified into 31 clusters representing different cell types within major cell lineages (Supplementary Figure S1B). A full list of canonical and signature marker genes for each cluster is provided in Supplementary Table S3.

2.4.5 | scRNA-seq signature score

For gene scoring analysis, different gene signatures in subpopulations were compared using the Seurat AddModuleScore function [21]. The immunosuppressive signature score was defined as the average expression of a series of immune checkpoint inhibitors [25] and immunosuppressive molecules [16], while the dysfunctional signature score [26] was defined as the average expression of a set of genes related to T cell dysfunction. In addition, the cytotoxic signature score was defined as the mean expression of genes that translated to effector cytotoxic proteins and well-described cytotoxic T cell activation markers. A list of immune co-stimulatory molecules [25, 27] associated with Treg function and a list of transcription factors (TFs) [28] related to the T cell exhaustion have also been provided in Supplementary Table S4, alongside genes included in the signatures mentioned above.

2.4.6 | Differential expression and Gene Ontology (GO) enrichment analysis

To identify cell cluster-specific differentially expressed genes (DEGs), two-sided unpaired Wilcoxon tests were performed on all the expressed genes (expressed in at least 20% of cells in either cluster of cells) by using the Seurat FindAllMarkers function. Cell type-specific signature marker genes were selected and visualized with a dot heatmap plot or stacked violin plot. Gene expression feature plots were generated by FeaturePlot, in which each cell was colored based on the expression level of the selected gene. The top 50 highly expressed genes of each cluster are shown in the heatmap plot. Cell cluster-specific DEGs with an absolute average fold change > 1.5 and adjusted *P*-values < 0.05 were chosen, and the mitochondrial genes or ribosomal genes were excluded for downstream enrichment analysis. Additionally, the FindMarkers function was used to calculate TNBC-specific genes, i.e., TNBC *vs.* $HER2^+$, TNBC *vs.* Luminal, and TNBC *vs.* Normal. A two-sided unpaired Wilcoxon test was used for genes expressed by ≥ 10% of cells in either group. Based on the differential expression from the single-cell gene expression data, significant enriched GO terms were then acquired for each cluster using the R package clusterProfiler (version 4.1.4) [29].

2.4.7 | Developmental trajectory inference

To determine potential lineage differentiation between different B cell populations, trajectory analysis was performed using the Monocle 2 (version 2.18.0) [30] algorithm. A CellDataSet object was created using the newCellDataSet function with expressionFamily set to be negbinomial size. Dimensionality reduction was performed with the DDRTree algorithm and max_components parameters = 4, using the expression of the top 3,000 highly variable genes detected as described above. The cell trajectory was then captured using the orderCells function and the inferred cell trajectories were visualized by the plot_cell_trajectory function. To visualize genes whose expression levels changed along with the pseudotime trajectory, the plot_pseudotime_heatmap function was used, using genes with adjusted *P*-value < 0.01, fold change > 1.5, and belonging to the TFs. To detect genes that play an important role in cell fate decisions, the branched expression analysis modeling was implemented to identify genes with branch-dependent expression. The plot_genes_branched_heatmap function was used to visualize genes with branch-dependent expression, where the genes were selected as either q value < 0.05 and belonging to TFs, or q value $< 1 \times 10^{-6}$ and belonging to the top 3,000 highly variable genes. These genes were also used for GO enrichment analysis.

2.4.8 | Cell-cell ligand-receptor communication analysis

The CellChat (version 1.1.3) [31] R package was used to identify and visualize the intercellular communication networks between T cells and B cells from scRNA-seq data. The package contained 1,939 pairs of well-curated ligand and receptor pairs, including 1,199 pairs of secreted signaling interactions, 319 pairs of cell-cell contact

interactions, and 421 pairs of extracellular matrix receptor interactions. Interactions and interaction strength among different breast cancer groups were calculated, and the overall information flow of each signaling pathway was compared. The minimum number of cells required for cell-cell communication analysis in each cell group was set to 10. Significant cellular communication pairs with $P < 0.05$ were extracted, and the TNBC-specific pathways were also extracted. That is, there was a significant interaction only in the TNBC subtype but not in the other groups. All of the significant interactions (ligand-receptor pairs) were then identified for a list of TNBC-specific pathways, and their average expression among different cell subtypes was visualized by the ComplexHeatmap (version 2.6.2) [32] R package. For a given pair of a ligand and receptor, a violin plot was used to visualize their expression levels across groups and samples.

2.5 | Survival analyses with gene signatures

Public gene expression and survival data from the Molecular Taxonomy of Breast Cancer International Consortium (METABRIC) [33] dataset were accessed using the cBioPortal public datahub (https://github.com/cBioPortal/datahub) [34]. The TNBC samples were defined as $HER2^-$, ER^-, and PR^-, and samples with missing values were removed ($n = 293$). The public validation dataset was downloaded from the Gene Expression Omnibus database (https://www.ncbi.nlm.nih.gov/geo/) with the accession number GSE31519, and a total of 383 TNBC samples with available survival data were included in the analysis.

The calculation of the specific cell cluster signature score was as follows. First, cell cluster-specific genes were defined as those significantly upregulated in the specific cell cluster compared to the other clusters, i.e., adjusted P-value < 0.01, fold change ≥ 1.5, delta percentage $\geq 15\%$, while excluding mitochondrial/ribosomal/long non-coding RNA/microRNA genes. Second, the cell cluster-specific signature score was calculated by averaging the expression of cell cluster-specific genes after weighting their log2 fold change. Finally, the infiltration level of the specific cell cluster in the METABRIC and GSE31519 cohorts was evaluated by the cell cluster signature score as the continuous variable.

Multivariate Cox regression analyses were utilized to screen predictors identified by univariate analyses and select an optimal prognostic model based on the Akaike information criterion (AIC) method. Multivariable Cox analyses were adjusted by lymph node status, tumor size, age at diagnosis, and histological grade. The prognosis risk score was defined by a combination of selected predictors weighted by their Cox regression β coefficients. Kaplan-Meier survival curves were generated by partitioning cases in a 1:1 split based on the ranked signature expression. All survival analyses and hazard ratio (HR) calculations were performed using the survival R package (version 3.2-11), with survival curves visualized using the survminer R package (version 0.4.9). Univariate and multivariate Cox analysis results were visualized as forest plots via the forestplot R package (version 1.10.1).

2.6 | External validation in scRNA-seq dataset

The scRNA-seq data (GSE176078) was utilized to validate our main findings. The GSE176078 was a scRNA-seq dataset included a total of 26 breast cancer samples that were collected from 5 treated patients and 21 naïve patients. The scRNA-seq data derived from the 21 untreated samples was used to validate our results, including 7 TNBC, 4 $HER2^+$ and 10 luminal-like breast cancer samples.

2.7 | Visualization and statistical analysis

The GO enrichment results were visualized as dot or bar plots by the ggplot2 (version 3.3.5) R package. The bar plot and pie plot were also generated by the ggplot2 (version 3.3.5) R package. Protein-protein interaction (PPI) networks were extracted from the STRING database (https://cn.string-db.org/) [35, 36], preserving active credible interaction that excluded text mining interaction sources. The PPI network was visualized by Cytoscape software (version 3.8.2) [37]. Heatmaps were generated by the ComplexHeatmap (version 2.6.2) R package [32]. The Ridge plot was visualized by the ggridges (version 0.5.3) R package. Unpaired two-sided Wilcoxon rank-sum tests were used for pair-wise comparisons. Statistical significance was accepted for $P < 0.05$. For all differential expression and gene set testing analyses, P-values were corrected for multiple testing using the Benjamini-Hochberg protocol. All statistical analyses were performed in R (version 4.0.5).

3 | RESULTS

3.1 | Cohort characterization and single-cell profiling of the immune cells in breast cancer

A cohort of female patients ($n = 17$) who were diagnosed with invasive ductal breast cancer and underwent mastectomy were enrolled in this study (Figure 1A). The median age of patients within this cohort was 61 years (ranging from 33 to 73 years). Lymph node positivity was

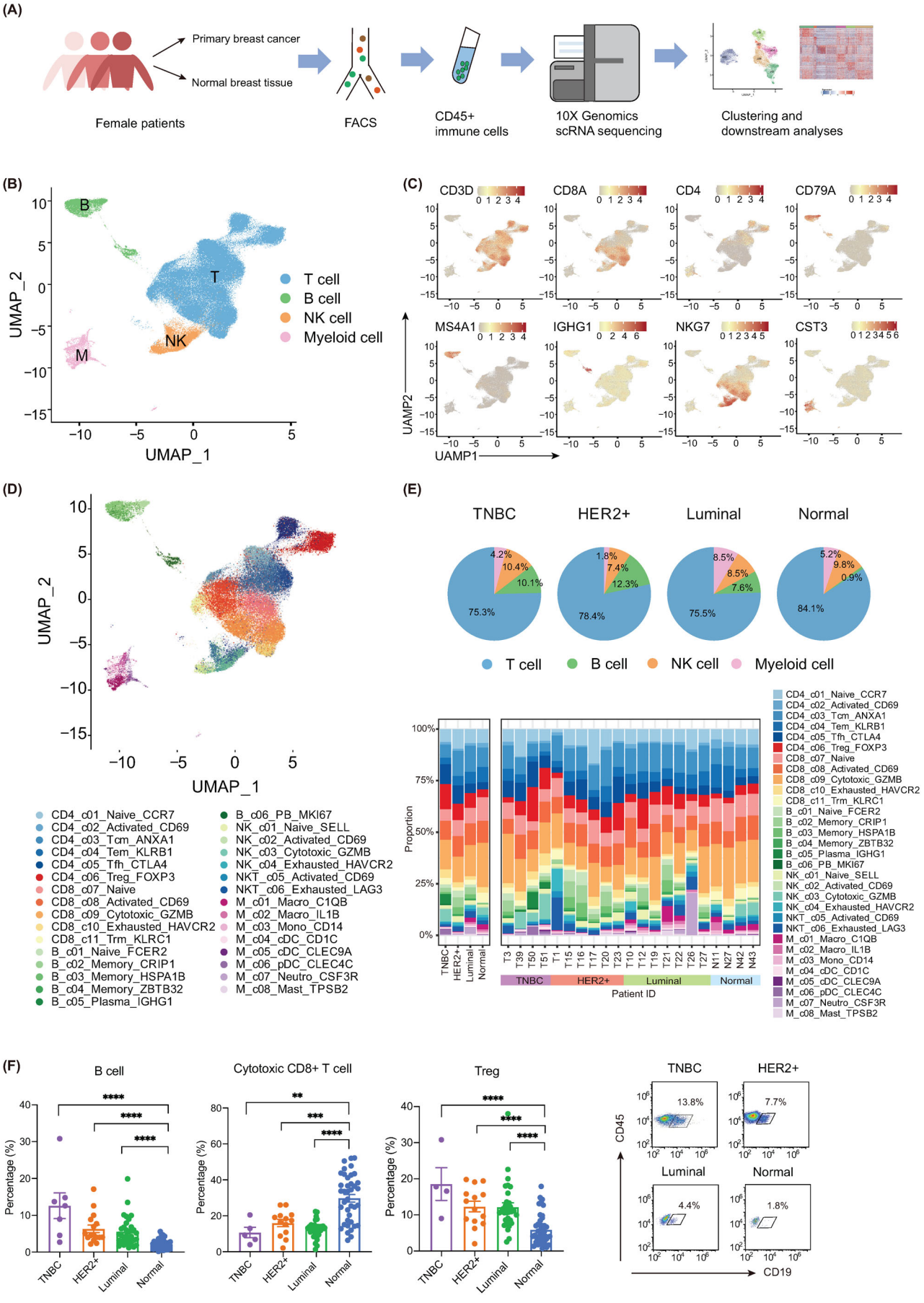

identified in 40% of patients and 60% of patients were classified as histological grade III. For molecular subtype, there were 4 patients with TNBC, 6 with HER2$^+$, and 7 with luminal-like breast cancer in this cohort. Detailed clinicopathological characteristics are listed in Supplementary Table S1. To elucidate the immune landscape of breast cancer with different molecular subtypes, scRNA-seq was performed on CD45$^+$ immune cells isolated by FACS from a panel of 21 freshly resected breast tissue samples in this cohort: 4 normal mammary tissues, 4 TNBC, 6 HER2$^+$, and 7 luminal-like breast cancer (Figure 1A). A total of 117,958 high-quality single-cell transcriptomes of these immune cells were obtained (66.6% from tumor tissues and 33.4% from normal tissues) (Supplementary Figure S1A, Supplementary Table S2).

As shown in Figure 1B, 4 major immune cell clusters, including T cells, B cells, NK cells, and myeloid cells, were distinguished by examining canonical marker genes when projecting cells into a 2D UMAP plot (Figure 1C, Supplementary Table S3). By unsupervised clustering, these 4 cell populations were further partitioned into 31 immune cell subpopulations: 11 T cell clusters, 6 B cell clusters, 6 NK cell clusters, and 8 myeloid cell clusters (Figure 1D, Supplementary Figure S1B).

To unravel the heterogeneity of the immune cell atlas in breast cancer, proportions of major cell populations and subpopulations among different subtypes of breast cancer and normal tissues were compared (Supplementary Tables S5-8). Of note, B cells were predominantly enriched in TNBC, HER2$^+$, and luminal-like breast cancer, but were scarce in normal tissues, with average proportions of 10.1%, 12.3%, and 7.6%, versus 0.9%, respectively (Figure 1E, Supplementary Figure S1C). Flow cytometry on independent tumor and normal samples was performed to validate the findings of scRNA-seq. Similarly, there were fewer B cells in normal tissues compared to those in TNBC, HER2$^+$, and luminal-like breast cancer tissues (Figure 1F). Regarding subpopulations, a lower level of GZMB$^+$ cytotoxic CD8$^+$ T cells was found, but a higher level of FOXP3$^+$ Tregs in tumors compared to normal tissues was found, indicating a suppressive TIME in breast cancer (Figure 1E). These findings were also confirmed by flow cytometry, which showed that the proportion of cytotoxic CD8$^+$ T cells was significantly increased, whereas the proportion of Tregs significantly decreased, in normal tissues compared to in tumor tissues (Figure 1F, Supplementary Figure S1D).

3.2 | Immunosuppressive environment mediated by T cells in TNBC

It was identified here that T cells constitute the largest infiltrating immune cell cluster in breast cancer. After re-clustering 93,115 T cells, a total of 11 T cell clusters were identified based on their signature genes, including 6 clusters in the CD4$^+$ compartment and 5 clusters in the CD8$^+$ compartment (Figures 2A–C, Supplementary Figure S2A, Supplementary Table S9). CD4_c01_Naive_CCR7 highly expressed "naïve" marker genes, such as *CCR7* and *SELL*. CD4_c05_follicular helper T (Tfh)_CTLA4 was characterized by high expression of the *CXCL13*, *CTLA4*, *BATF*, and *PDCD1*. CD4_c06_Treg_FOXP3 specifically expressed "Treg" marker genes, such as *FOXP3* and *IL2RA*. A group of "cytotoxic" marker genes (*NKG7*, *PRF1*, *GZMB*, and *GZMK*) was highly expressed in CD8_c09_Cytotoxic_GZMB, while CD8_c10_Exhausted_HAVCR2 was featured by "exhaustion" marker genes, including *TIGIT*, *CTLA4*, *PDCD1*, *LAG3*, and *HAVCR2*. The functional features of each cluster were indicated by GO enrichment analyses, and the cytotoxic and dysfunctional signature scores further confirmed the annotation for these clusters (Supplementary Figures S2B-C, Supplementary Table S10). Notably, the distribution pattern of the T cell clusters was heterogeneous across various molecular subtypes of breast cancer (Figure 2D). Compared with HER2$^+$

FIGURE 1 Immune cell landscape in different subtypes of breast cancers and normal tissues. (A) Flow chart of the overall study design and analytic workflow. (B) UMAP showed 4 major immune cell clusters, including T cells, B cells, NK cells, and myeloid cells, from breast cancers (BC, $n = 17$) and normal tissue ($n = 4$). (C) Expression of canonical marker genes used to determine the major clusters (T cells: CD3D, CD8A, and CD4; B cells: CD79A, MS4A1, and IGHG1; NK cells: NKG7; myeloid cells: CST3). (D) UMAP of the 31 detailed immune cell clusters of 117,958 cells derived from BC patients and normal tissues. Cell clusters were named based on cluster-specific gene expression patterns. (E) Proportions of 4 major cell clusters (upper: pie charts) and 31 detailed cell clusters (lower: bar plots) in TNBC ($n = 4$), HER2$^+$ BC ($n = 6$), luminal-like BC ($n = 7$) and normal tissues ($n = 4$). (F) Left panel: Proportions of B cells, cytotoxic CD8 T cells, and Treg cells across different molecular subtypes of breast cancers and normal tissues in flow cytometry (Panel B cells: TNBC, $n = 7$; HER2$^+$ BC, $n = 16$; luminal-like BC, $n = 31$; normal tissues, $n = 38$. Panel cytotoxic CD8 T cells: TNBC, $n = 5$; HER2$^+$ BC, $n = 13$; luminal-like BC, $n = 32$; normal tissues, $n = 39$. Panel Treg cells: TNBC, $n = 4$; HER2$^+$ BC, $n = 14$; luminal-like BC, $n = 32$; normal tissues, $n = 43$.) Data are presented as the mean ±SEM. P values were calculated using the Mann-Whitney U test. **, $P < 0.01$; ***, $P < 0.001$; ****, $P < 0.0001$. Right panel: representative flow cytometry graphs of B cells across different molecular subtypes of breast cancers and normal tissues. Abbreviations: UMAP, uniform manifold approximation and projection; BC, breast cancer; TNBC, triple negative breast cancer; HER2$^+$, human epidermal growth factor receptor 2-positive; FACS, fluorescence-activated cell sorting; Treg, regulatory T; SEM, standard error of mean; IFN-γ, interferon-γ.

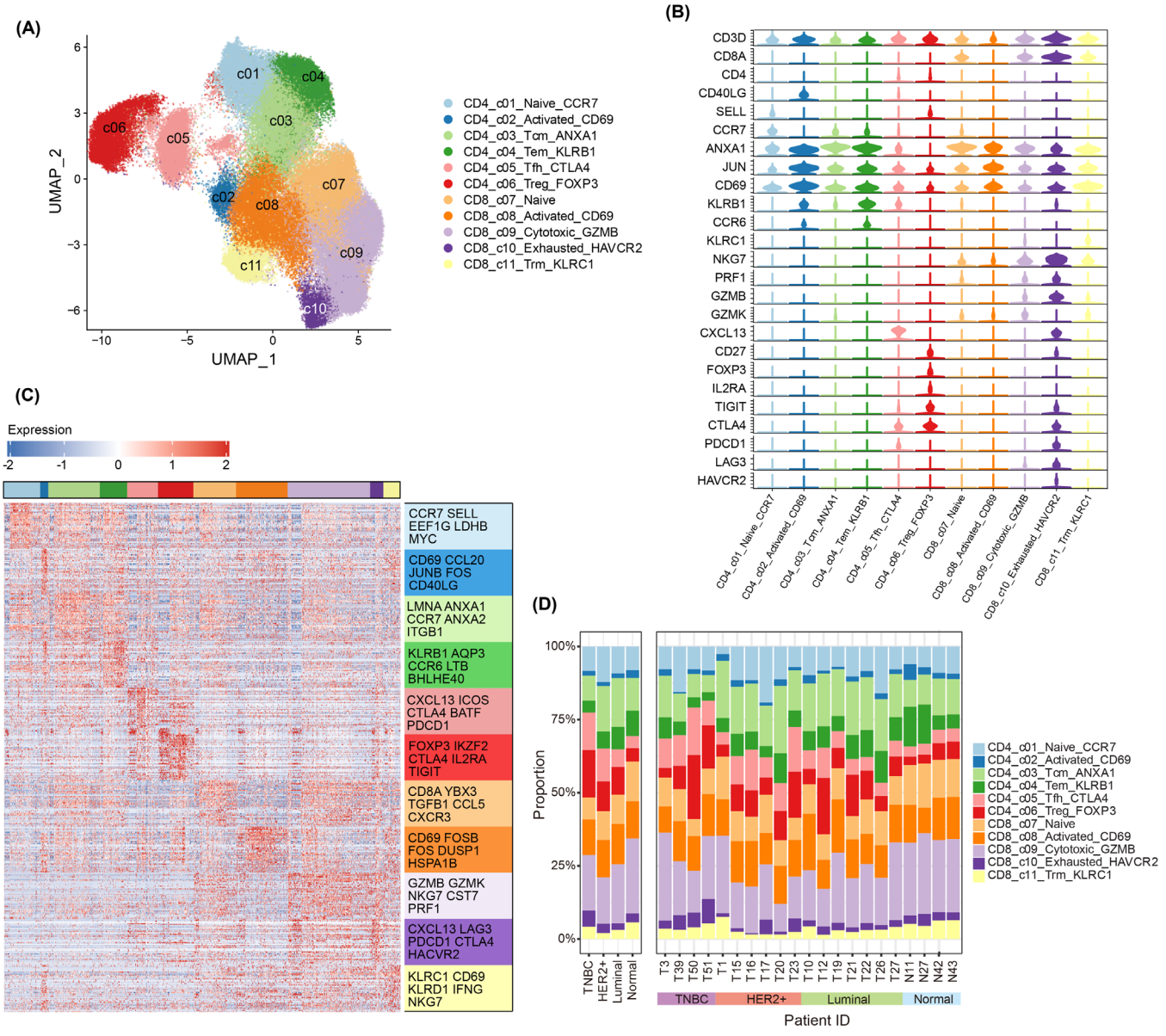

and luminal-like breast cancers, increased levels of Tregs (CD4_c06_Treg_FOXP3) and exhausted CD8$^+$ T cells (CD8_c10_Exhausted_HAVCR2) were found in TNBC, indicating an immunosuppressive environment (Supplementary Figure S2D). The higher infiltrating levels of Tregs and exhausted CD8$^+$ T cells in TNBC were also validated in the external scRNA-seq dataset (GSE176078, Supplementary Figure S2E).

It has been widely acknowledged that T cells in the tumor microenvironment are inclined to become exhausted or suppressed by Tregs, which impedes the T cell-mediated killing of tumor cells [38]. Thus, here, the transcriptomic features of Tregs (CD4_c06_Treg_FOXP3), cytotoxic CD8$^+$ T cells (CD8_c09_Cytotoxic_GZMB), and exhausted CD8$^+$ T cells (CD8_c10_Exhausted_HAVCR2) were further dissected (Supplementary Table S11). Transcriptome analyses of Tregs indicated that co-stimulation genes of *LGALS9*, *TNFRSF4*, *CD27*, and *CD28* as well as immunosuppression-related genes of *IL2RA*, *IL2RB*, *IL2RG*, *ENTPD1*, and *LAG3* were enriched in TNBC compared to those in HER2$^+$ and luminal-like breast cancer, suggesting that Tregs in TNBC harbor a more significant immunosuppressive function (Figure 2E). Similarly, compared to HER2$^+$ and luminal-like breast cancer, exhausted CD8$^+$ T cells and cytotoxic CD8$^+$ T cells in TNBC expressed a higher level of dysfunctional signature genes, such as *CXCL13*, *CCL3*, *TIGIT*, *LAG3*, *HACVR2*, and *ENTPD1*, as well as TFs related to exhaustion, such as *IFI16*, *IKZF3*, *ZNF683*, *PRDM1* and *RBPJ*, indicating a higher degree of exhaustion in CD8$^+$ T cells in TNBC (Figure 2E). Consistent with the results of gene expression analyses, the distinct immunosuppressive features of T cells in TNBC were also reflected by the significantly higher immunosuppression signature score of the Tregs and the higher dysfunctional signature score of the exhausted CD8$^+$ T cells and cytotoxic CD8$^+$ T cells (Figure 2F). Collectively, these results demonstrated that TNBC has a distinct T cell-mediated immunosuppression environment with enrichment of Tregs and exhausted CD8$^+$ T cells as a feature, as well as a more prominent suppressive function of Tregs and exhaustion tendency of both cytotoxic and exhausted CD8$^+$ T cells.

3.3 | Enrichment of plasma cells in TNBC

As the cell population with the most pronounced differences in in terms of proportion between tumors and normal tissues, B cells were further partitioned into 6 subpopulations, each with its unique signature genes (Figures 3A-D, Supplementary Table S9). B_c01_Naive_FCER2 specifically expressed "naïve" marker genes, such as *IGHD* and *FCER2*, and B_c04_Memory_ZBTB32 highly expressed *ZBTB32* and *TNFRSF1B*. B_c05_Plasma_IGHG1 was characterized by the high expression of genes related to antibody secretion (*IGHG4*, *IGHG1*, *JCHAIN*, *MZB1*, *XBP1*, and *PRDM1*). Besides genes related to antibody secretion, B_c06_PB_MKI67 also highly expressed proliferation genes, such as *MKI67*, *TOP2A*, and *UBE2C*, thus, representing proliferating plasmablast. Next, based on the DEGs from each cluster, the functional characteristics of different B cell clusters were further explored (Supplementary Figure S3A, Supplementary Table S10). B_c05_Plasma_IGHG1 was highly associated with the regulation of complement activation and Fc-γ receptor signaling pathway, which are both related to humoral immunity. B_c06_PB_MKI67 was mainly enriched in the ATP metabolic process and oxidative phosphorylation, reflecting high energy consumption due to its active proliferation. These findings further validated the annotations for B cell clusters. When comparing the proportions of each B cell cluster across different molecular subtypes, it was found that TNBC exhibited a drastically higher level of plasma cells (B_c05_Plasma_IGHG1) than HER2$^+$ and luminal-like breast cancers (48.2%, 1.5%, and 4.0%, respectively; Figure 3E, Supplementary Figure S3B), which was further confirmed by external validation in scRNA-seq dataset (GSE176078, Supplementary Figure S3C) and flow cytometry analyses (Figure 3F, Supplementary Figure S3D).

To determine the differentiation trajectory of B cell clusters, pseudotime analyses were performed. The pseudotime trajectory of B cells preserved two differentiation pathways (Figure 4A), starting with naïve B cells and ending mostly with the memory B cells at one terminus, or the plasma cells and plasmablast at the other (Figure 4B).

FIGURE 2 Compositions and functions of T cells in different molecular subtypes of breast cancer and normal tissues. (A) UMAP visualization of the 11 T cell clusters. (B) Stacked violin plot displaying the expression of selected marker genes in 11 T cell clusters. (C) Heatmap of top 50 DEGs in each T cell cluster. (D) Bar plots presenting the proportions of 11 T cell clusters in different breast cancer molecular subtypes (left panel) and samples (right panel). (E) Heatmap showing the expression pattern of selected genes in Treg cells (left panel), exhausted CD8 T cells (middle panel), and cytotoxic CD8 T cells (right panel) across different breast cancer molecular subtypes. (F) Violin plot comparing the signature scores in Treg cells (left panel), exhausted CD8 T cells (middle panel), and cytotoxic CD8 T cells (right panel) across different breast cancer molecular subtypes. *P* values were calculated using the Mann-Whitney U test. ****, $P < 0.0001$. Abbreviations: UMAP, Uniform manifold approximation and projection; TNBC, triple negative breast cancer; HER2$^+$, human epidermal growth factor receptor 2-positive; DEG, differentially expressed gene; Treg, regulatory T cell.

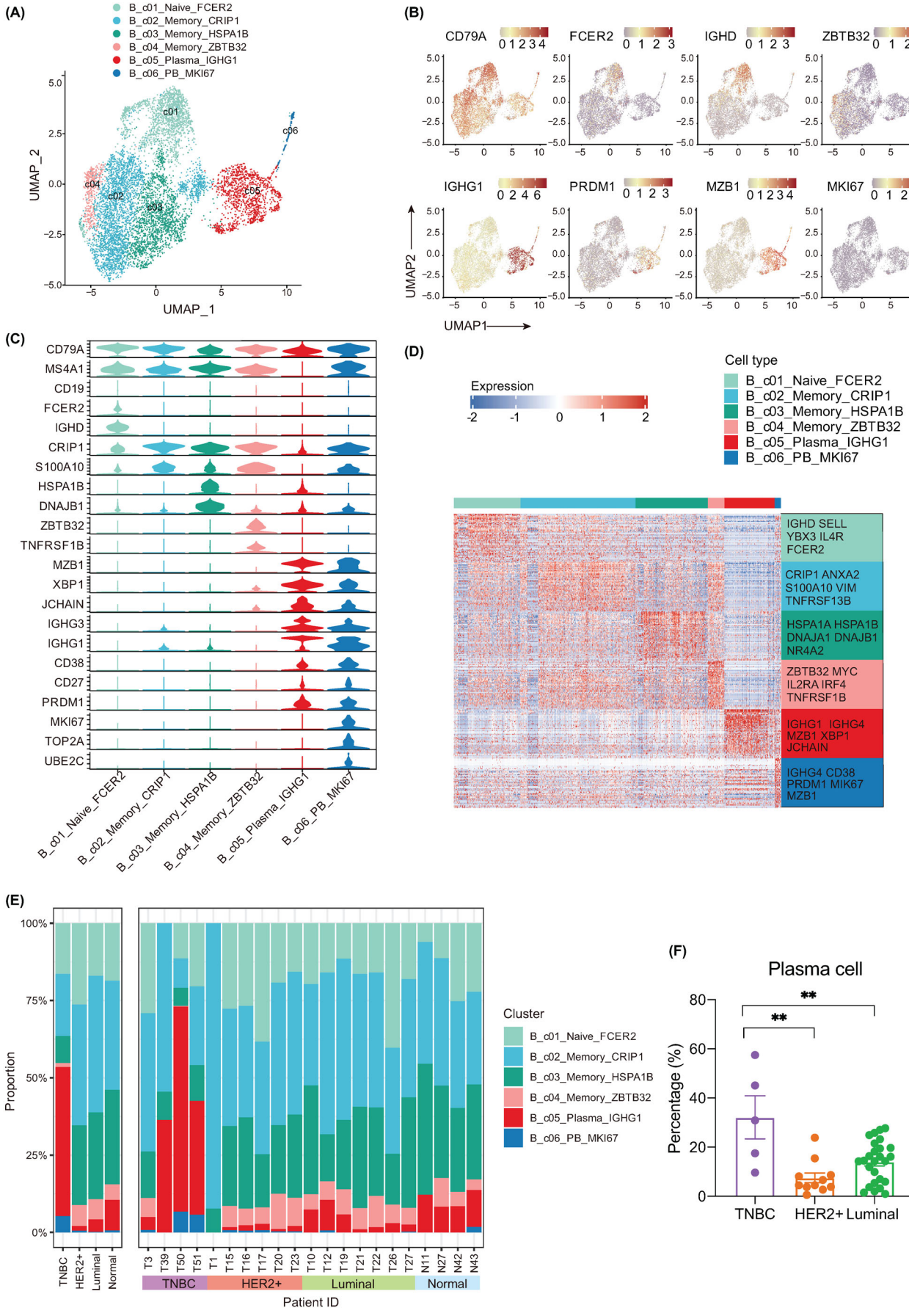

Although cells belonging to the same clusters could be distributed into different differentiation pathways, analyses showed a continuous transition process from naïve B cells to memory B cells to finally ending with plasmablast and plasma cells, according to the pseudotime order (Figure 4C). Alongside this transition process, "naïve" marker gene expression levels (*IGHD* and *FCER2)* significantly decreased, while genes related to proliferation (*MKI67*, *TOP2A*, and *UBE2C*) and antibody secretion (*IGHG1*, *IGHG3*, *JCHAIN*, *PRDM1*, and *XBP1*) exhibited an increased level of expression with the emergence of plasma cells and plasmablast (Figure 4C). Differentially expressed TFs along this transition process, such as *BCL6*, *IRF4*, and *E2F5*, were also displayed in Figure 4C, and might be key players in the differentiation process.

According to the position in the trajectory branch, B cells were divided into three groups, termed as Pre-branch, Path I, and Path II (Figure 4D). About 75.1% of naïve B cells were defined as Pre-branch. The majority of memory B cells were located in Path I, with memory B cells (B_c04_Memory_ZBTB32) constituting the highest proportion (89.8%). Nevertheless, nearly all plasma cells and plasmablast were grouped into Path II, with proportions of 95.2% and 92.0%, respectively. Interestingly, the two-path differentiation mode existed in all subtypes of breast cancer, but the differentiation pattern varied (Figure 4D). B cells in TNBC tended to differentiate from Pre-branch to Path II, with 82.7% of B cells distributed in Path II and 4.4% of B cells distributed in Path I. In contrast, B cells in HER2$^+$ and luminal-like breast cancers were more likely to differentiate from Pre-branch to Path I rather than Path II, with only 8.1% and 11.5% of B cells located in Path II, respectively (Figure 4D, Supplementary Figure S4A).

Signature genes and enriched GO pathways for Pre-branch, Path I and Path II were identified (Figure 4E, Supplementary Figure S4B, Supplementary Tables S12-14). Cells in Path I highly expressed several genes encoding heat shock proteins (HSPs), such as Hsp70 members (*HSPA1* and *HSPA8*) [39] and Hsp90 members (*HSP90AA1*and *HSP90AB1*) [40], which acted as important immunomodulators in antigen presentation and T cell activation [41]. Cells in Path II highly expressed the genes associated with antibody synthesis and humoral immunity, such as *XBP1* [42] and *MZB1* [43], and genes encoding immunoglobulins. In addition, PPI network analyses based on differentially expressed TFs of each path suggested that some genes might be the key regulatory TFs in B cell differentiation, such as *STAT1* in Path II, *MYC* in Path I and *JUN* in Pre-branch (Supplementary Figure S4C). Furthermore, different gene expression patterns were also observed along the two different trajectory paths (Figure 4F). Along with the cellular trajectory of B cells from Pre-branch to Path I, the expression levels of genes related to T cell differentiation and leukocyte cell-cell adhesion were gradually elevated (Figure 4F, Supplementary Tables S12-14). On the other hand, along with the cellular trajectory of B cells from Pre-branch to Path II, increased expression of genes enriched in B cell activation, immunoglobulin mediated immune response, and the Fc-γ receptor signaling pathway was observed (Figure 4F, Supplementary Tables S12-14).

Overall, these results indicated that B cells in TNBC exhibited distinct differentiation patterns compared to other molecular subtypes. Specifically, B cells in TNBC tended to differentiate into plasma cells and plasmablasts, exerting the effect of humoral immunity. However, B cells in HER2$^+$ and luminal-like breast cancers were more likely to differentiate into memory B cells, exerting the effect of T cell activation.

3.4 | Distinct T cell-B cell crosstalk in TNBC

To determine the potential mechanism driving the above-mentioned distinct T and B cell infiltration patterns in TNBC, the expression levels of ligand-receptor pairs in 11 T cell clusters and six B cell clusters were investigated to predict T cell-B cell interactions. A total of 229 functionally related signaling pathways composed of 2,021 validated molecular interactions were analyzed. The results showed that 26 signaling pathways were active in T cell-B cell crosstalk but the composition and relative strength of these signaling pathways varied by molecular subtype (Supplementary Figure S5A, Supplementary Tables S15-16). Specifically, the *CD86* and *CD39* signaling pathways were specifically active in TNBC, while the *CXCL* signaling

FIGURE 3 Heterogeneity of B cell subsets among different breast cancer molecular subtypes and normal tissues. (A) UMAP visualization of the 6 B cell clusters. (B) UMAP plots showing the expression of selected marker genes on 6 B cell clusters. (C) Stacked violin plot showing the expression level of selected marker genes in each B cell cluster. (D) Heatmap of top 50 DEGs across 6 B cell clusters. (E) Bar plot showing the proportions of 6 B cell clusters in different breast cancer molecular subtypes (left panel) and samples (right panel). (F) Proportions of plasma cells in tumor-infiltrating B cells across different breast cancer molecular subtypes in flow cytometry (TNBC, $n = 5$; HER2$^+$ breast cancer, $n = 11$; luminal-like breast cancer, $n = 26$). Data are presented as the mean ± SEM. *P* values were calculated using the Mann-Whitney U test. **, $P < 0.01$. Abbreviations: UMAP, Uniform manifold approximation and projection; TNBC, triple negative breast cancer; HER2$^+$, human epidermal growth factor receptor 2-positive; DEG, differentially expressed gene.

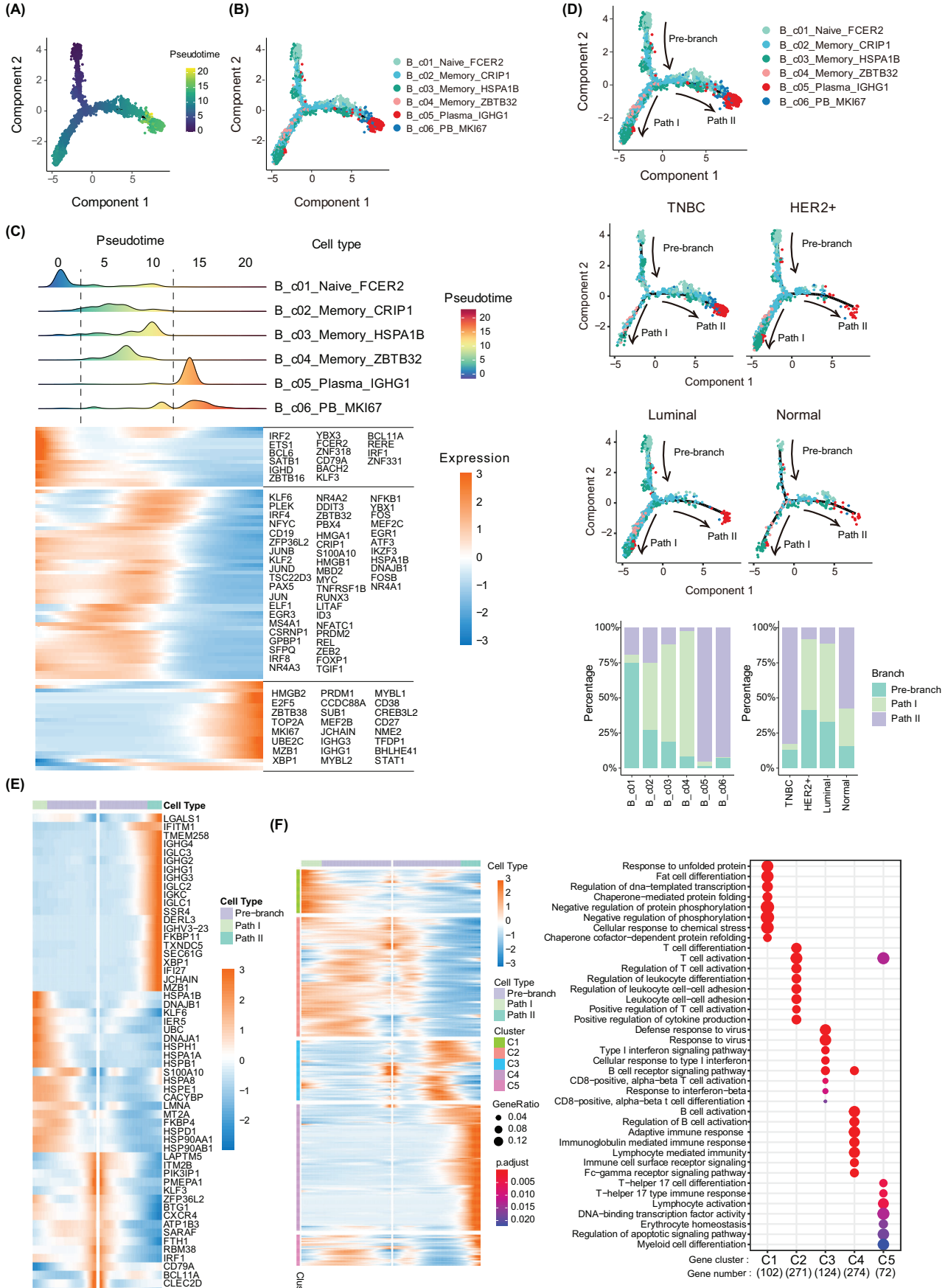

pathways were predominantly derived from HER2$^+$ breast cancer. Pathways that were significantly more prominent in TNBC were then systemically investigated and screened for, of which the T cell-B cell interactions based on 29 ligand-receptor pairs were mostly enriched between memory B cells (B_c04_Memory_ZBTB32), plasmablasts (B_c06_PB_MKI67), CTLA4$^+$ Tfh (CD4_c05_Tfh_CTLA4), Tregs (CD4_c06_Treg_FOXP3), and exhausted CD8$^+$ T cells (CD8_c10_Exhausted_HAVCR2) (Figure 5A).

By evaluating the communication probability (Figure 5B) and ligand-receptor pair expression level (Figures 5C-D, Supplementary Figure S5B) of interactions with an immunoregulatory function, 7 TNBC-enriched T cell-B cell interactions were finally identified among the 5 clusters that may facilitate the distinct TIME in TNBC, which are highlighted in the cord diagram (Supplementary Figure S5C). It was found that the IL16-CD4 pair was highly expressed between B_c06_PB_MKI67 and CD4_c06_Treg_FOXP3 in TNBC. As previous studies have shown that IL-16 can recruit Tregs [44, 45], in the present study, it was hypothesized that plasmablasts are more likely to attract Tregs into the TIME of TNBC. Moreover, plasmablasts (B_c06_PB_MKI67 were also predicted to interact with exhausted CD8$^+$ T cells (CD8_c10_Exhausted_HAVCR2) via the *LGALS9-HAVCR2* pair in TNBC in this study (Figures 5B-C). This interaction may cause an increased level of exhausted T cells because it has been reported that LGALS9 negatively regulated Th1 cell responses by binding to HAVCR2, resulting in the induction of T cell apoptosis and exhaustion [46, 47]. In addition, the strong *CD27-CD70* interactions in TNBC identified in our analyses may facilitate T cell exhaustion (Figures 5B-C), as the persistent delivery of costimulatory signals via CD27-CD70 interactions could exhaust the T cell pool according to the previous study [48]. Besides, Tregs (CD4_c06_Treg_FOXP3) and exhausted CD8$^+$ T cells (CD8_c10_Exhausted_HAVCR2) showed strong potential interaction with memory B cells (B_c04_Memory_ZBTB32) by ligand-receptor pairs *ICOSLG-CTLA4* and *CD86-CTLA4* in TNBC, which might also contribute to the suppressive TIME (Figures 5B-C). Moreover, it has been previously reported that CD39 could turn extracellular ATP into extracellular adenosine (ADO), which could combine its receptor ADORA2A to actuate immunosuppressive TME [49]. As an exclusive signaling pathway in TNBC, the CD39 signaling pathway enables the communication of memory B cells (B_c04_Memory_ZBTB32) with exhausted CD8$^+$ T cells (CD8_c10_Exhausted_HAVCR2) via the *ENTPD1 (CD39)-ADORA2A* pair, which could promote the immunosuppression in TNBC as well (Figures 5B-C).

Here, memory B cells (B_c04_Memory_ZBTB32) in TNBC highly expressed *ICOSLG* and *CXCR5*, while Tfh cells (CD4_c05_Tfh_CTLA4) in TNBC highly expressed *ICOS* and *CXCL13* (Figure 5D). A previous study revealed that ICOSLG expressed by B cells could regulate T cell-B cell signal exchange within the germinal center, thereby promoting B cells to become long-term antibody-producing plasma cells [50]. It has also been reported that CXCL13-producing Tfh cells could be chemoattracted by CXCR5$^+$ B cells to form the germinal center, further promoting the differentiation of memory B cells to plasma cells [51]. Therefore, the prominent ICOSLG-ICOS interaction and CXCL13-CXCR5 interaction between B_c04_Memory_ZBTB32 and CD4_c05_Tfh_CTLA4 in TNBC may have formed a positive cycle that promotes plasma cell differentiation unique to TNBC, which would explain the high proportion of plasma cells in TNBC.

Together, the specific T cell-B cell crosstalk in TNBC based on *IL16-CD4*, *LGALS9- HAVCR2*, *CD27-CD70*, *ICOSLG-CTLA4*, *CD86-CTLA4*, and *ENTPD1 (CD39)-ADORA2A* pairs was attributed to the immunosuppressive TIME, while the prominent *ICOSLG-ICOS* and *CXCL13-CXCR5* interaction helps the TIME build a favorable environment for B cells to differentiate into plasma cells (Figure 5E).

3.5 | Prognostic signature based on T cell-B cell crosstalk in TNBC

As the results of this study suggested that T cell-B cell crosstalk might help to shape the distinct TIME in TNBC,

FIGURE 4 Pseudotime analysis defines two differentiation patterns of B cells in different molecular subtypes of breast cancer. (A) Pseudotime trajectory of B cells. (B) Distribution of B cell subsets in the trajectory graph. (C) Ridge distribution of B cell subsets (upper panel) along pseudotime and heatmap of the expression level of selected marker genes and transcriptional factors (lower panel) along the pseudotime. (D) Identification of different paths in trajectory analyses of B cells (total: upper panel; different groups: middle panel) and proportions of different B cell paths in each cluster and group (lower panel) (E) Pseudotemporal gene-expression profiles of the top 20 (by fold change) DEGs of each path. Columns are points in pseudotime, rows are genes, and the beginning of pseudotime is in the middle of the heatmap. (F) Pseudotemporal gene expression profile along two branches. Left panel: The heatmap of DEGs along with the pseudotime from Pre-branch to Path I or Path II, which were clustered hierarchically. Right panel: The top GO terms enriched in each gene cluster. Abbreviations: TNBC, triple negative breast cancer; HER2$^+$, human epidermal growth factor receptor 2-positive; DEG, differentially expressed gene; GO, Gene Ontology.

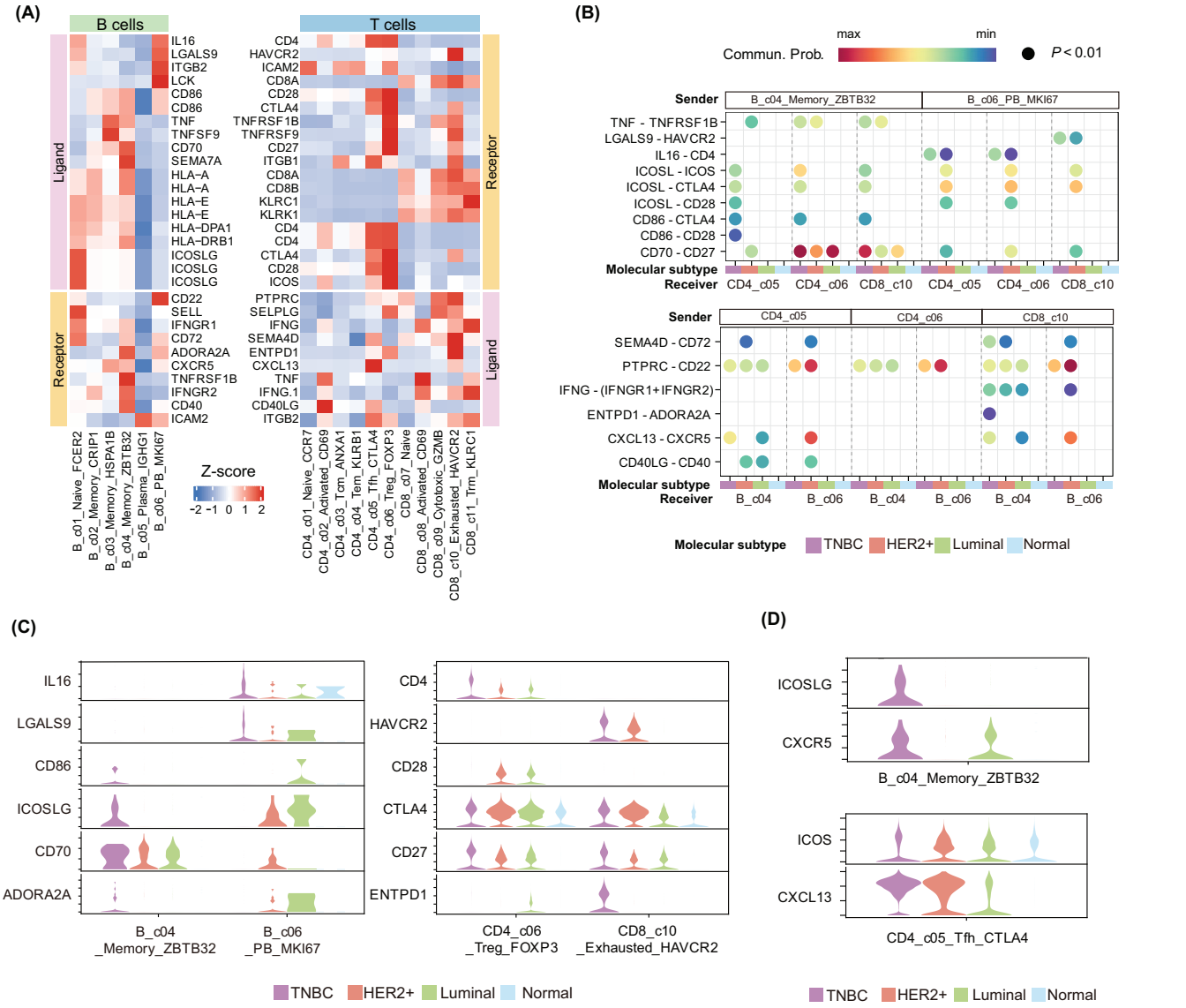

it was hypothesized that relevant genes and cell clusters involved in the T cell-B cell crosstalk might provide significant prognostic information for patients with TNBC. Therefore, a prognostic signature was generated based on T cell-B cell crosstalk in TNBC.

Firstly, the prognostic value of the involved genes and cell clusters in the METABRIC dataset was evaluated, where DEGs-based single-cell-derived gene signatures were used to estimate the infiltrating level of distinct cell clusters (Supplementary Table S17). The results indicated that *CTLA4*, *ICOS*, *CXCL13*, CD4_c05-Tfh_CTLA4, CD4_c06_Treg_FOXP3, CD8_c10_exhausted_HAVCR2, and B_C04_memory_ZBTB32 were significantly related to the relapse-free survival (RFS) and overall survival (OS) in patients with TNBC (Figure 6A, Supplementary Figure S6A). Secondly, according to multivariate Cox regression analysis based on the above seven predictors, the TBCS was constructed with three selected predictors, namely *CTLA4*, CD4_c06_Treg_CTLA4, and B_c04_memory_ZBTB32. The TBCS for each patient's calculation was as follows: (−0.534 × *CTLA4*) + (1.152 × CD4_c06_Treg_FOXP3 score) + (−1.805 × B_c04_memory_ZBTB32 score). Afterward, the prognosis between the high- and low-risk group divided by the risk score of the patients with TNBC in the METABRIC dataset and an external validation dataset (GSE31519) was compared to validate the prognostic value of TBCS (Figure 6B, Supplementary Figure S6B). Patients in the high-risk group had significantly worse RFS (P = 0.000,75) and OS (P = 0.000,59) in the METABRIC dataset and worse RFS in the external validation dataset (P = 0.023; Figure 6C). After adjusting for age, tumor size, lymph node status, and tumor grade (Figure 6D), patients with TNBC in the high-risk group had a worse prognosis compared to those in the low-risk group for both RFS (HR = 1.800; 95% confidence intervals [CI], 1.240-2.613; P = 0.002) and OS (HR = 1.620; 95% CI, 1.170-2.242; P = 0.004). However, TBCS failed to predict the prognosis in patients with HER2$^+$ breast cancer (P > 0.05) or luminal-like breast cancer (P > 0.05), suggesting that the unique prognostic value of TBCS was particularly beneficial for patients with TNBC (Supplementary Figure S6C).

3.6 | Enrichment of cytotoxic NK cells and plasmacytoid dendritic cells in TNBC

Besides T and B cells, the distribution patterns of NK and myeloid cells in TNBC were also found to differ from those of other molecular subtypes of breast cancer. A total of 10,676 NK cells were re-clustered into 6 subsets, including 4 NK clusters and 2 NKT clusters (Figures 7A-D; Supplementary Tables S9-10). NK_c03_Cytotoxic_GZMB exhibited elevated expression levels of the "cytotoxic" marker genes (*GZMB*, *GZMA*, and *CST7*), and DEGs of this cluster were mainly associated with oxidative phosphorylation and the ATP metabolic process, suggesting its exuberant biological activity. NK_c04_Exhausted_HAVCR2 that highly expressed *HAVCR2*, an exhausted marker gene, was related to negative regulation of the immune system process and negative regulation of cell killing, indicating its exhausted state. Both NKT_c05_Activated_CD69 and NKT_c06_Exhausted_LAG3 highly expressed the T cell marker gene (*CD3G*) and NK cell marker gene (*GNLY* and *NKG7*), thus were annotated as NKT cells.

Interestingly, similar to normal tissues, TNBC exhibited comparably high levels of cytotoxic NK cells but low levels of exhausted NK cells, representing an NK-active antitumor environment. In contrast, HER2$^+$ and luminal-like breast cancers were enriched with exhausted NK cells but had few cytotoxic NK cells, indicating their NK-exhausted protumor environment (Figure 7E). This disparate NK cell infiltration pattern indicated that patients with TNBC may not benefit from NK-targeted therapy due to the relatively high level of cytotoxic NK cells at baseline, potentially limiting the capabilities of drugs to further strengthen the antitumor effect of NK cells. Nevertheless, NK-based immunotherapy is suggested for the development of suitable treatments for HER2$^+$ and luminal-like breast cancers due to their NK-exhausted microenvironment.

Likewise, myeloid cells were further partitioned into 8 subclusters based on their signature genes (Supplementary Figures S7A-D, Supplementary Table S9). Two kinds of macrophages were identified: M_c01_Macro_C1QB, which highly expressed *C1QB* and *APOE*, and M_c02_Macro_IL1B, which highly expressed

FIGURE 5 Cell-cell communication analysis indicates unique T cell-B cell interactions in TNBC. (A) Heatmap showing the expression level of ligand-receptor pairs within TNBC-significant cell communications in the overall population. (B) Comparison of the significant ligand-receptor pairs across different subtypes. Dot color represents the communication probability of the specific ligand-receptor pair between sender cluster and receiver cluster. (C) Violin plot showing the expression level of ligand-receptor pairs associated with significant signaling pathways in TNBC which indicates B cells could help to construct the immunosuppressive microenvironment dependent on T cells. (D) Violin plot showing the expression level of ligand-receptor pairs associated with significant T cell-B cell crosstalk existed in TNBC that may facilitate the differential of B cells to plasma cells. (E) Summarization of representative TNBC-significant T cell-B cell crosstalk that might modulate its distinct immunoenvironment. The ligand is written as the former and the receptor as the latter followed by a dash. Cell type that expresses each gene is noted by the color. The arrows on the line point to the receptors. Abbreviations: TNBC, triple negative breast cancer; HER2$^+$, human epidermal growth factor receptor 2-positive.

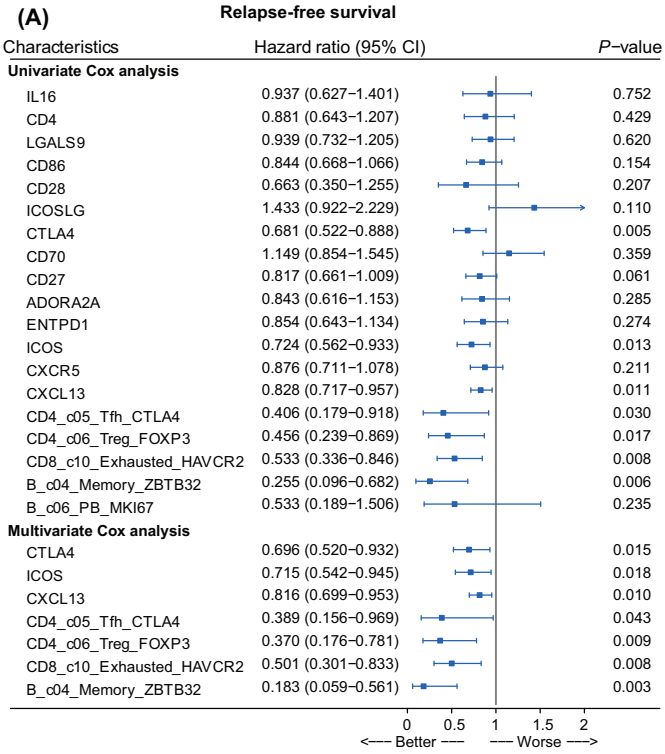

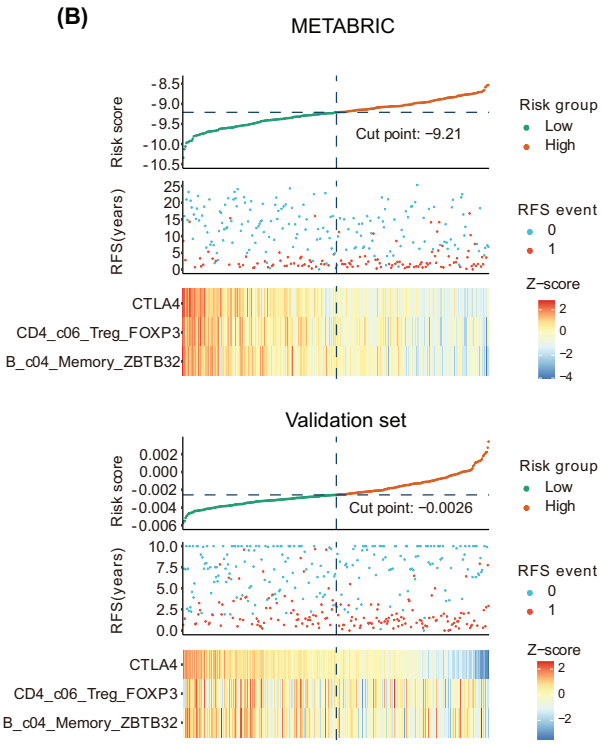

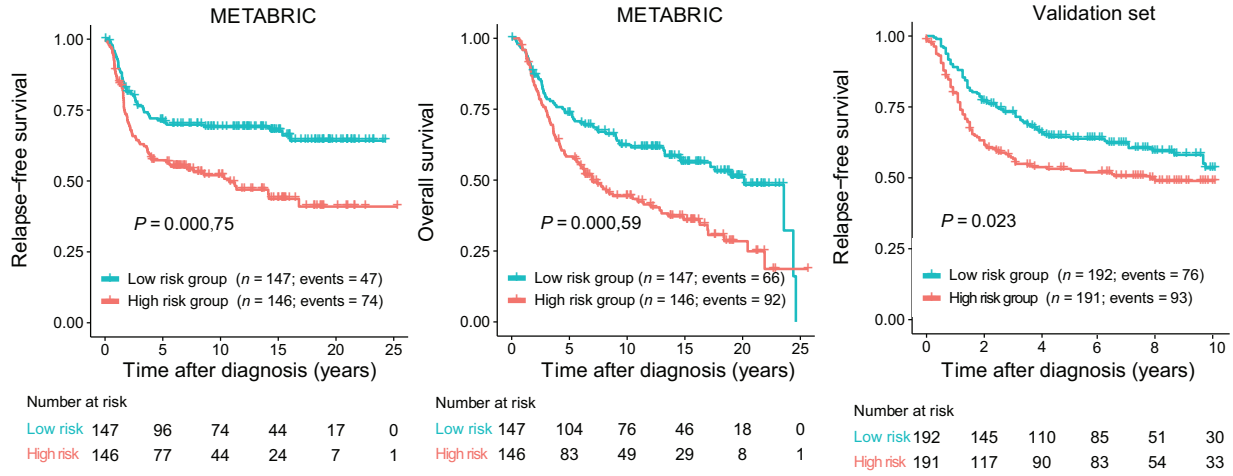

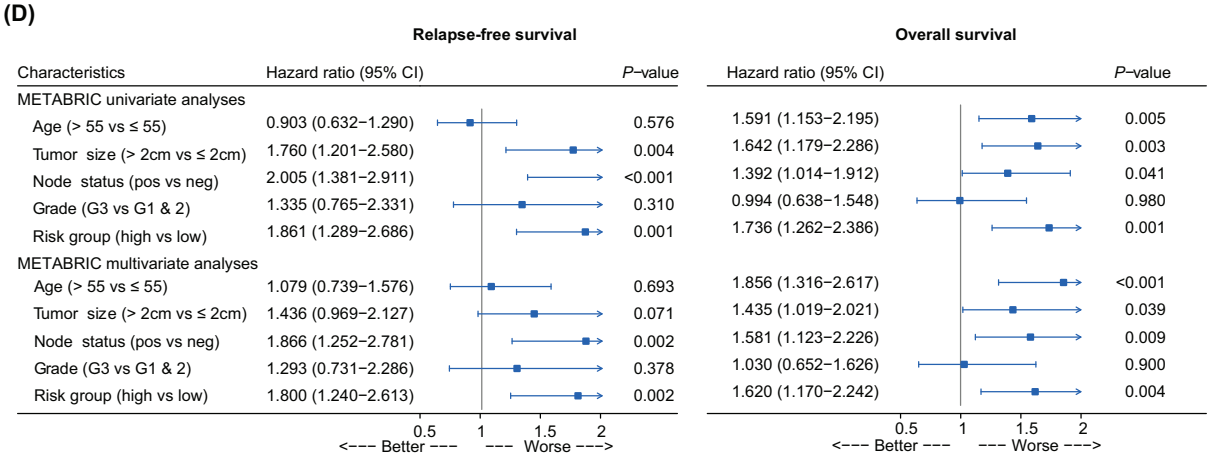

IL1B and *FCN1*. In addition, monocytes featured by *CD14*, *FCN1*, and *S100A9*; neutrophils featured by *FCGR3B* and *CSF3R*; mast cells featured by *TPSB2* and *CPA3*; and three dendritic cell (DC) clusters, including two classic DCs (M_c04_cDC_CD1C and M_c05_cDC_CLEC9A) and one plasmacytoid DC (pDC, M_c06_pDC_CLEC4C), were identified and were consistent with their functional enrichment results (Supplementary Figure S7E, Supplementary Table S10). The distribution pattern of M subclusters varied considerably across different molecular subtypes of breast cancer (Supplementary Figure S7F). Compared to HER2$^+$ and luminal-like breast cancer, TNBC featured an increased level of pDC, which has been reported to contribute to breast cancer progression and a poor overall prognosis [52, 53], indicating that targeting pDC may be an attractive therapeutic strategy to overcome tumor immune tolerance for TNBC.

4 | DISCUSSION

Understanding the TIME is of great significance for improving disease prognosis and guiding immunotherapy, but the characterization of the immune landscape in TNBC compared with that of luminal-like and HER2$^+$ breast cancer remains limited. In this study, it was found that TNBC has a distinct immunosuppressive TIME feature as reflected by the enrichment of Tregs and exhausted CD8$^+$ T cells, and its companion B cells tend to differentiate to plasma cells, which is potentially driven by T cell-B cell crosstalk. The TBCS was further generated for the prediction of TNBC prognosis.

Characterizing T cell infiltration and its functions provides novel therapeutic targets for breast cancer. As is widely accepted, ICBs exert their antitumor effect by unleashing the cytotoxic CD8$^+$ T cells in the tumor environment [54], while the cytotoxic activities of these effector T cells could be suppressed by Tregs [55], restraining the efficiency of ICBs. Here, it was hypothesized that the low response to ICB in some patients with TNBC may partly be attributed to the enrichment of Tregs; thus, combination therapy depleting Tregs may improve the response rate in such patients. CD8$^+$ T cell exhaustion is potentially another factor hindering the immunotherapy effect [56]. As found in the present study, the exhausted CD8$^+$ T cell level was enriched in TNBC, and a fraction of cytotoxic CD8$^+$ T cells appeared to be in a transition state to exhaustion, indicating their constrained tumor-cytotoxic activity. Therefore, preventing cytotoxic CD8$^+$ T cells from reaching exhaustion or reactivating exhausted CD8$^+$ T cells might be a possible therapeutic strategy in TNBC, which has already gained increasing attention from researchers and yielded fruitful results [57, 58]. Collectively, the appropriate immunotherapy strategy for TNBC should aim at effective immunosuppression reversal by depleting or inhibiting Tregs, preventing T cell exhaustion, and invigorating exhausted T cells, which warrants further exploration in the future.

Tumor-infiltrating lymphocytes exert great influence on tumor growth and the immunotherapy response, while the role of B cells in solid tumors is understood to a much lesser extent compared to that of T cells. Current opinions hold that B cells could exert both protumor and antitumor effects, depending on their phenotype, secreted antibodies, and the surrounding TME [59]. On the one hand, B cells could protect against tumors by producing antibodies to mediate antibody-dependent cell cytotoxicity and by presenting tumor-derived antigens to T cells to initiate antitumor immunity. On the other hand, B cells could promote tumor progression by releasing immunosuppressive cytokines, which facilitate the development of Tregs and the immunosuppressive phenotype of myeloid cells [60, 61]. The controversial prognostic role of B cells has been reported in different tumor types. High levels of B and plasma cells are related to an improved prognosis in melanoma, lung adenocarcinoma [62], and non-small cell lung cancer [63], whereas they are correlated with poor survival outcomes in glioblastoma and renal cell carcinoma [64]. In breast cancer, conflicting evidence exists for the prognostic role of B cells and plasma cells, with some studies reporting an association with a worse prognosis [65, 66], and others suggesting an association with a

FIGURE 6 Construction of prognostic signature based on unique T cell-B cell interactions in TNBC. (A) Prognostic value of specific genes and cluster signature for RFS in METABRIC TNBC patients. Forest plot showing HR and 95% CI derived from univariate and multivariate Cox analyses adjusted for age, tumor size, node status, and tumor grade. Within the forest plot, HR for each variable is depicted as a box, and 95% CIs are shown as horizontal lines. The vertical line crossing the value of 1 represents a non-statistically significant effect, and odds greater than one indicate worse effects. (B) Distribution of risk score, relapse status, the expression level of genes, and cell cluster signature involved in the prognostic model among TNBC patients in METABRIC (upper panel) and external validation set (lower panel). (C) Kaplan-Meier curves of RFS or OS between low-risk patients and high-risk patients in METABRIC TNBC patients (left and middle panels) and external validation set (right panel), indicating that high-risk patients had a significantly poor prognosis. (D) Predictive performance of the prognostic signature according to univariate and multivariate Cox analyses adjusted by age, tumor size, node status, and grade, suggesting the signature was an independent predictor for RFS and OS. Abbreviations: RFS, relapse-free survival; OS, overall survival; HR, hazard ratio; CI, confidence interval; TNBC, triple negative breast cancer.

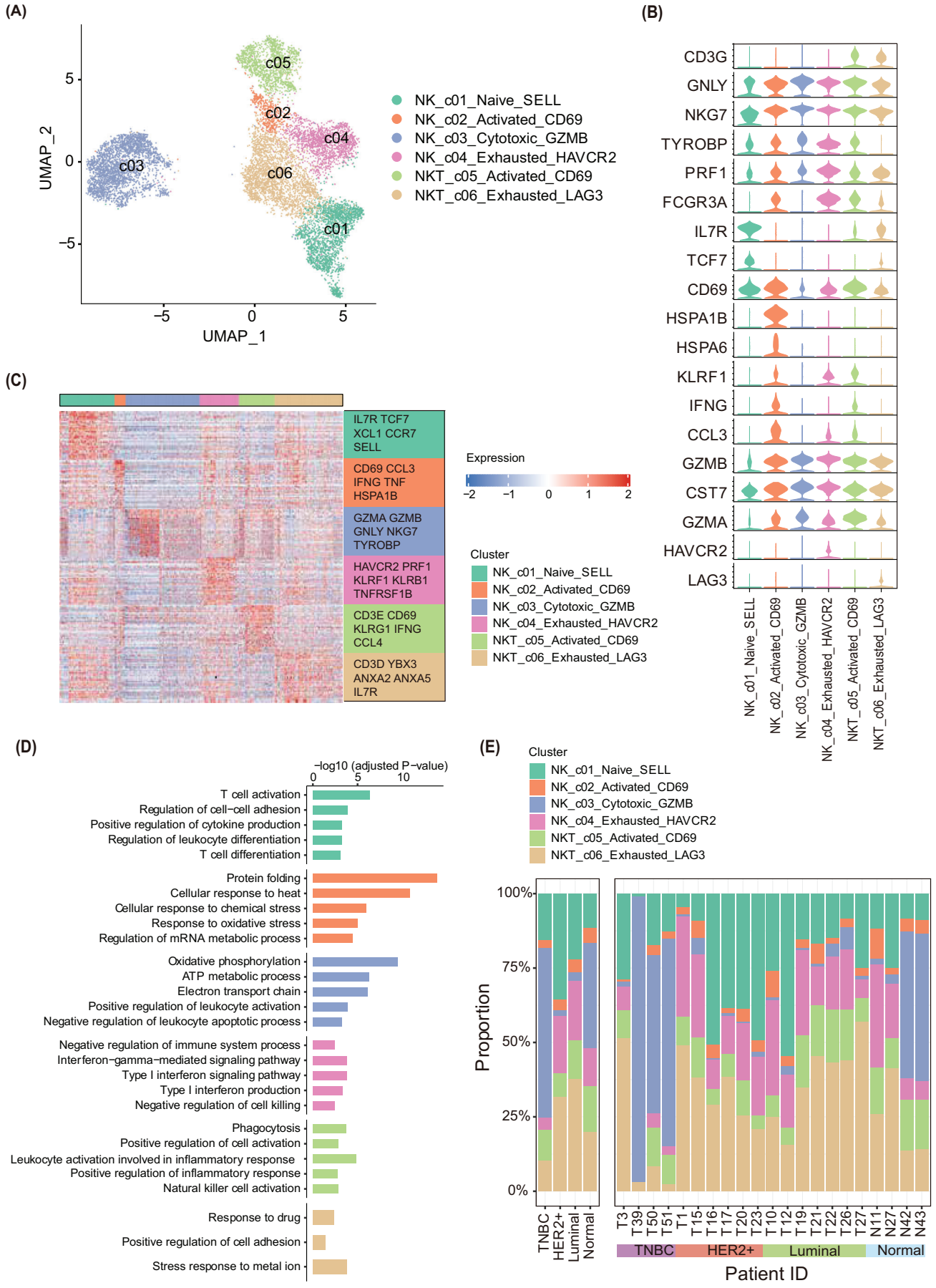

better prognosis [67, 68]. These controversial results may be attributed to the heterogeneity of B cell subsets and functions in different types of breast cancer. Here, the single-cell portrait of B cells was thoroughly investigated, and the enrichment of plasma cells was revealed in TNBC for the first time at the single-cell level. It was also found that B cells tend to differentiate to plasma cells, which is promoted by interplay between B cells and T cells, which may contribute to the T cell-mediated immunosuppressive feature in TNBC. The potential role of plasma cells as prognostic factors or predictive biomarkers and as agents or targets of immunotherapy in TNBC requires further investigation.

Recently, the importance of T cell-B cell interactions in tumor immunity has attracted increased attention. Several T cell-B cell crosstalk mediated by cytokines or direct interactions have been revealed, which suppress antitumor T cell responses and contribute to immune suppression [69]. It has been found that immunosuppressive B cells can interact with T cells via the PD-1/PD-L1 pathway, leading to the attenuation of T cell activation [70]. It has also been found that tumor-infiltrating B cells may restrain T cell responses via the interaction between OX40L on B cells and OX40 on T cells in various murine solid tumors such as EL4 thymoma and MC38 colon cancer [71]. Besides inhibiting antitumor T cell responses, potentiating the local expansion of Tregs is another mechanism of T cell-B cell interactions to induce immunosuppression. For example, regulatory B cells (Bregs) have been reported to promote the proliferation of Tregs through interactions between CD5 and CD27, which, in turn, induce the development of Bregs [72]. In the present study, a unique T cell-B cell crosstalk pattern enriched in TNBC was identified. This finding, combined with previous reports on specific ligand-receptor pair function, resulted in the hypothesis that the unique T cell-B cell crosstalk may lead to greater Treg infiltration and $CD8^+$ T cell exhaustion as well as plasma cell differentiation. These T cell-B cell interactions not only help to establish the TBCS to predict the prognosis for TNBC but also pave the way for future therapeutic approaches to remodel the TIME by targeting this unique T cell-B cell crosstalk pattern or synergistic combinations of immunotherapies.

As an independent prognostic factor for TNBC, the TBCS refined the risk stratification for patients with TNBC. Several immune-related genes or immune cell populations have been reported to be capable of providing prognostic information for breast cancer, such as the $CD8^+$ TRM signature [15], naïve B signature, and Bmem signature [16]. However, the combinational prognostic signature integrating the single-gene expression level with the cell cluster infiltration level evaluated by the cell cluster signature score derived from scRNA-seq data was put forward for the first time, to our knowledge, in the present study. The candidate prognostic genes and cell clusters for TBCS were selected based on unique T cell-B cell crosstalk in TNBC, which could help to cultivate a distinct immune microenvironment according to this study's analyses. Therefore, the TBCS may reflect the whole picture of immunity status in breast cancer, thus, enabling it to provide comprehensive and reliable prognostic information.

NK cells play important roles in the innate immune responses against tumors and represent an emerging target for tumor immunotherapies. Nevertheless, the characteristics of NK cells so far have been poorly addressed in breast cancer at the single-cell level. In this study, it was found that TNBC has a relatively higher infiltration level of cytotoxic NK cells as compared to that of the other two subtypes of breast cancer, suggesting that a limited benefit can be obtained from NK cell-based immunotherapy for TNBC. Conversely, rather than cytotoxic NK cells, the exhausted NK cells were enriched in $HER2^+$ and luminal-like breast cancers, which makes these two subtypes with a poor response to ICBs potential ideal candidates for NK cell-based immunotherapy. Collectively, the findings of this study not only highlighted the different features of various molecular subtypes of breast cancer but also provided NK-based immunotherapy as a promising research direction for retarded development in $HER2^+$ and luminal-like breast cancer.

One limitation of this study lay in the limited sample size for scRNA-seq, especially upon assigning to different molecular subtypes. The study design for sequencing isolated immune cells made the sample preparation more difficult because of the low immune infiltration in breast cancer. However, the major findings of the immune cell infiltration level of different molecular subtypes of breast cancer were further confirmed by flow cytometry in additional samples and the published scRNA-seq dataset, which increased the credibility of the conclusions of this study to some extent. Another limitation of the study was the lack of single-cell transcriptomic data of tumor

FIGURE 7 $HER2^+$ and luminal-like BC display different features in NK cells infiltration compared to TNBC. (A) Distributions of the 6 NK cell subsets in the UMAP plot. (B) Stacked violin plot of the expression of selected marker genes in each NK cluster. (C) Heatmap of top 50 DEGs across 6 NK cell clusters. (D) Bar plots exhibiting top 5 GO enrichment terms of DEGs from each cluster. (E) Bar plots presenting the proportions of 6 NK cell clusters in different molecular subtypes (left panel) and samples (right panel). Abbreviations: UMAP, Uniform manifold approximation and projection; NK, natural killer; TNBC, triple negative breast cancer; $HER2^+$, human epidermal growth factor receptor 2-positive; DEGs, differentially expressed genes; GO, Gene Ontology.

cells, which limited the prediction to cell-cell interactions between tumor and immune cells. Previous studies have mentioned that tumor mutations could influence T cell infiltration and function in the microenvironment, which is worth further exploration [73]. The present study focused on the immunomodulatory role of immune cells but fell short of exploring the possible capabilities and mechanisms of tumor cells in remodeling the immune microenvironment. However, performing scRNA-seq on immune cells isolated from samples improved the sequencing depth of the immune cells, which enabled the presentation of a more detailed depiction of the immune landscape in different molecular subtypes of breast cancer. The lack of experimental validation on the function of specific T cell-B cell crosstalk was also a limitation. Combined with the findings of cell-cell communication analyses and previous reports on specific ligand-receptor pair functions, it was hypothesized that the distinct TIME of TNBC may be driven by unique T cell-B cell crosstalk, which requires further experimentation to confirm.

5 | CONCLUSIONS

The present study comprehensively characterized the distinct immune landscape of TNBC in comparison with that of $HER2^+$, luminal-like breast cancer, and normal breast tissues by single-cell profiling. TNBC has a unique TIME featuring T cell-mediated immunosuppression and an abundance of plasma cells, potentially shaped by T cell-B cell interactions. A TBCS was established to predict the prognosis for patients with TNBC. Furthermore, the findings of this study provide insight into the potential targets for future immunotherapy strategies in different molecular subtypes of breast cancer.

DECLARATIONS

AUTHOR CONTRIBUTIONS

Conceptualization: Kunwei Shen, Yichuan Xiao, Qiang Tian, and Xiaosong Chen, Sample collection and preparation for sequencing: Shuning Ding and Qingchen Zhu, Single-cell RNA sequencing: Shengyue Wang, Flow cytometry experiments and data analyses: Shuning Ding and Qingchen Zhu, Bioinformatics analysis, data management and visualization: Niu Qiao, Bioinformatic investigation: Niu Qiao, Shuning Ding, Qingchen Zhu, and Yiwei Tong, Funding acquisition: Kunwei Shen and Yichuan Xiao, Supervision: Kunwei Shen, Yichuan Xiao, Qiang Tian, and Xiaosong Chen, Writing – original draft: Shuning Ding, Niu Qiao, and Qingchen Zhu, Writing – review and editing: Kunwei Shen, Yichuan Xiao, Qiang Tian, and Xiaosong Chen.

ACKNOWLEDGMENTS

Not applicable.

CONFLICT OF INTEREST STATEMENT

The authors declare that they have no competing interests.

FUNDING

This study was supported by the National Natural Science Foundation of China (82072937), National Natural Science Foundation of China (82072897), National Natural Science Foundation of China (82002773), Shanghai Municipal Education Commission-Gaofeng Clinical Medicine Grant Support (20172007), Science and Technology Commission of Shanghai Municipality Shanghai Sailing Program (21YF1427400), and Beijing Breast Disease Society.

ETHICS APPROVAL AND CONSENT TO PARTICIPATE

This study was approved by the Ethics Committee of Ruijin Hospital, Shanghai Jiao Tong University School of Medicine (ID: 2020-332). The tissue samples were obtained with written informed consent from each patient.

CONSENT FOR PUBLICATION

Not applicable.

DATA AVAILABILITY STATEMENT

All data in the study are available from corresponding authors upon reasonable request. Custom scripts for analyzing data are available upon request. Visualization and custom exploration of scRNA-seq data are available at https://mikaqiao.shinyapps.io/scBC/.

ORCID

Shuning Ding https://orcid.org/0000-0003-4938-5354
Xiaosong Chen https://orcid.org/0000-0002-0036-9444

REFERENCES

1. Wang Y, Wang M, Wu HX, Xu RH. Advancing to the era of cancer immunotherapy. Cancer Commun (Lond). 2021;41(9):803–29.
2. Dent R, Trudeau M, Pritchard KI, Hanna WM, Kahn HK, Sawka CA, et al. Triple-negative breast cancer: clinical features and patterns of recurrence. Clin Cancer Res. 2007;13(15 Pt 1):4429–34.
3. Haffty BG, Yang Q, Reiss M, Kearney T, Higgins SA, Weidhaas J, et al. Locoregional relapse and distant metastasis in conservatively managed triple negative early-stage breast cancer. J Clin Oncol. 2006;24(36):5652–7.
4. Hong R, Xu B. Breast cancer: an up-to-date review and future perspectives. Cancer Commun (Lond). 2022;42(10):913-36.
5. Marra A, Viale G, Curigliano G. Recent advances in triple negative breast cancer: the immunotherapy era. BMC Med. 2019;17(1):90.

6. Kwapisz D. Pembrolizumab and atezolizumab in triple-negative breast cancer. Cancer Immunol Immunother. 2021;70(3): 607–17.
7. Huober J, Barrios CH, Niikura N, Jarząb M, Chang YC, Huggins-Puhalla SL, et al. Atezolizumab With Neoadjuvant Anti-Human Epidermal Growth Factor Receptor 2 Therapy and Chemotherapy in Human Epidermal Growth Factor Receptor 2-Positive Early Breast Cancer: Primary Results of the Randomized Phase III IMpassion050 Trial. J Clin Oncol. 2022:Jco2102772.
8. Schmid P, Cortes J, Pusztai L, McArthur H, Kümmel S, Bergh J, et al. Pembrolizumab for Early Triple-Negative Breast Cancer. N Engl J Med. 2020;382(9):810–21.
9. Heeke AL, Tan AR. Checkpoint inhibitor therapy for metastatic triple-negative breast cancer. Cancer Metastasis Rev. 2021;40(2):537–47.
10. James JL, Balko JM. Biomarker predictors for immunotherapy benefit in breast: beyond PD-L1. Curr Breast Cancer Rep. 2019;11(4):217–27.
11. Sivapiragasam A, Ashok Kumar P, Sokol ES, Albacker LA, Killian JK, Ramkissoon SH, et al. Predictive Biomarkers for Immune Checkpoint Inhibitors in Metastatic Breast Cancer. Cancer Med. 2021;10(1):53–61.
12. Kolodziejczyk AA, Kim JK, Svensson V, Marioni JC, Teichmann SA. The technology and biology of single-cell RNA sequencing. Mol Cell. 2015;58(4):610-20.
13. Papalexi E, Satija R. Single-cell RNA sequencing to explore immune cell heterogeneity. Nat Rev Immunol. 2018;18(1): 35–45.
14. Chen H, Ye F, Guo G. Revolutionizing immunology with single-cell RNA sequencing. Cell Mol Immunol. 2019;16(3):242–9.
15. Savas P, Virassamy B, Ye C, Salim A, Mintoff CP, Caramia F, et al. Single-cell profiling of breast cancer T cells reveals a tissue-resident memory subset associated with improved prognosis. Nat Med. 2018;24(7):986–93.
16. Hu Q, Hong Y, Qi P, Lu G, Mai X, Xu S, et al. Atlas of breast cancer infiltrated B-lymphocytes revealed by paired single-cell RNA-sequencing and antigen receptor profiling. Nat Commun. 2021;12(1):2186.
17. Azizi E, Carr AJ, Plitas G, Cornish AE, Konopacki C, Prabhakaran S, et al. Single-Cell Map of Diverse Immune Phenotypes in the Breast Tumor Microenvironment. Cell. 2018;174(5):1293–308 e36.
18. Chung W, Eum HH, Lee HO, Lee KM, Lee HB, Kim KT, et al. Single-cell RNA-seq enables comprehensive tumour and immune cell profiling in primary breast cancer. Nat Commun. 2017;8:15081.
19. Wu SZ, Al-Eryani G, Roden DL, Junankar S, Harvey K, Andersson A, et al. A single-cell and spatially resolved atlas of human breast cancers. Nature Genetics. 2021;53(9): 1334–47.
20. Zheng GX, Terry JM, Belgrader P, Ryvkin P, Bent ZW, Wilson R, et al. Massively parallel digital transcriptional profiling of single cells. Nat Commun. 2017;8:14049.
21. Satija R, Farrell JA, Gennert D, Schier AF, Regev A. Spatial reconstruction of single-cell gene expression data. Nat Biotechnol. 2015;33(5):495–502.
22. McGinnis CS, Murrow LM, Gartner ZJ. DoubletFinder: Doublet Detection in Single-Cell RNA Sequencing Data Using Artificial Nearest Neighbors. Cell Syst. 2019;8(4):329–37 e4.
23. Korsunsky I, Millard N, Fan J, Slowikowski K, Zhang F, Wei K, et al. Fast, sensitive and accurate integration of single-cell data with Harmony. Nat Methods. 2019;16(12):1289–96.
24. Zappia L, Oshlack A. Clustering trees: a visualization for evaluating clusterings at multiple resolutions. Gigascience. 2018; 7(7).
25. Wykes MN, Lewin SR. Immune checkpoint blockade in infectious diseases. Nat Rev Immunol. 2018;18(2):91–104.
26. Li H, van der Leun AM, Yofe I, Lubling Y, Gelbard-Solodkin D, van Akkooi ACJ, et al. Dysfunctional CD8 T Cells Form a Proliferative, Dynamically Regulated Compartment within Human Melanoma. Cell. 2019;176(4):775–89 e18.
27. Li X, Wenes M, Romero P, Huang SC, Fendt SM, Ho PC. Navigating metabolic pathways to enhance antitumour immunity and immunotherapy. Nat Rev Clin Oncol. 2019;16(7):425–441.
28. Hu H, Miao YR, Jia LH, Yu QY, Zhang Q, Guo AY. AnimalTFDB 3.0: a comprehensive resource for annotation and prediction of animal transcription factors. Nucleic Acids Res. 2019;47(D1):D33–D8.
29. Yu G, Wang LG, Han Y, He QY. clusterProfiler: an R package for comparing biological themes among gene clusters. OMICS. 2012;16(5):284–7.
30. Trapnell C, Cacchiarelli D, Grimsby J, Pokharel P, Li S, Morse M, et al. The dynamics and regulators of cell fate decisions are revealed by pseudotemporal ordering of single cells. Nat Biotechnol. 2014;32(4):381–6.
31. Jin S, Guerrero-Juarez C, Zhang L, Chang I, Myung P, Plikus M, et al. Inference and analysis of cell-cell communication using CellChat. Nat Commun. 2021; 17;12(1):1088.
32. Gu Z, Eils R, Schlesner M. Complex heatmaps reveal patterns and correlations in multidimensional genomic data. Bioinformatics. 2016;32(18):2847–9.
33. Curtis C, Shah SP, Chin SF, Turashvili G, Rueda OM, Dunning MJ, et al. The genomic and transcriptomic architecture of 2,000 breast tumours reveals novel subgroups. Nature. 2012;486(7403):346–52.
34. Cerami E, Gao J, Dogrusoz U, Gross BE, Sumer SO, Aksoy BA, et al. The cBio cancer genomics portal: an open platform for exploring multidimensional cancer genomics data. Cancer Discov. 2012;2(5):401–4.
35. Szklarczyk D, Franceschini A, Wyder S, Forslund K, Heller D, Huerta-Cepas J, et al. STRING v10: protein–protein interaction networks, integrated over the tree of life. Nucleic Acids Research. 2015;43(D1):D447–D52.
36. Szklarczyk D, Morris JH, Cook H, Kuhn M, Wyder S, Simonovic M, et al. The STRING database in 2017: quality-controlled protein–protein association networks, made broadly accessible. Nucleic Acids Research. 2017;45(D1): D362–D8.
37. Cline MS, Smoot M, Cerami E, Kuchinsky A, Landys N, Workman C, et al. Integration of biological networks and gene expression data using Cytoscape. Nat Protoc. 2007;2(10):2366–82.
38. Tanaka A, Sakaguchi S. Regulatory T cells in cancer immunotherapy. Cell Res. 2017;27(1):109–18.
39. Milani V, Noessner E, Ghose S, Kuppner M, Ahrens B, Scharner A, et al. Heat shock protein 70: role in antigen presentation and immune stimulation. Int J Hyperthermia. 2002;18(6):563–75.

40. Graner MW. HSP90 and Immune Modulation in Cancer. Adv Cancer Res. 2016;129:191–224.
41. Zininga T, Ramatsui L, Shonhai A. Heat Shock Proteins as Immunomodulants. Molecules. 2018;23(11):2846.
42. Wöhner M, Pinter T, Bönelt P, Hagelkruys A, Kostanova-Poliakova D, Stadlmann J, et al. The Xbp1-regulated transcription factor Mist1 restricts antibody secretion by restraining Blimp1 expression in plasma cells. Front Immunol. 2022;13:859598.
43. Andreani V, Ramamoorthy S, Pandey A, Lupar E, Nutt SL, Lämmermann T, et al. Cochaperone Mzb1 is a key effector of Blimp1 in plasma cell differentiation and β1-integrin function. Proc Natl Acad Sci U S A. 2018;115(41):E9630–e9.
44. Skundric DS, Cruikshank WW, Drulovic J. Role of IL-16 in CD4+ T cell-mediated regulation of relapsing multiple sclerosis. J Neuroinflammation. 2015;12:78.
45. McFadden C, Morgan R, Rahangdale S, Green D, Yamasaki H, Center D, et al. Preferential migration of T regulatory cells induced by IL-16. J Immunol. 2007;179(10):6439–45.
46. Yang R, Sun L, Li CF, Wang YH, Yao J, Li H, et al. Galectin-9 interacts with PD-1 and TIM-3 to regulate T cell death and is a target for cancer immunotherapy. Nat Commun. 2021;12(1):832.
47. Li H, Wu K, Tao K, Chen L, Zheng Q, Lu X, et al. Tim-3/galectin-9 signaling pathway mediates T-cell dysfunction and predicts poor prognosis in patients with hepatitis B virus-associated hepatocellular carcinoma. Hepatology. 2012;56(4):1342–51.
48. Tesselaar K, Arens R, van Schijndel GM, Baars PA, van der Valk MA, Borst J, et al. Lethal T cell immunodeficiency induced by chronic costimulation via CD27-CD70 interactions. Nat Immunol. 2003;4(1):49–54.
49. Moesta AK, Li XY, Smyth MJ. Targeting CD39 in cancer. Nat Rev Immunol. 2020;20(12):739–55.
50. Liu D, Xu H, Shih C, Wan Z, Ma X, Ma W, et al. T-B-cell entanglement and ICOSL-driven feed-forward regulation of germinal centre reaction. Nature. 2015;517(7533):214–8.
51. Gu-Trantien C, Migliori E, Buisseret L, de Wind A, Brohée S, Garaud S, et al. CXCL13-producing TFH cells link immune suppression and adaptive memory in human breast cancer. JCI Insight. 2017;2(11):e91487.
52. Sisirak V, Faget J, Gobert M, Goutagny N, Vey N, Treilleux I, et al. Impaired IFN-α production by plasmacytoid dendritic cells favors regulatory T-cell expansion that may contribute to breast cancer progression. Cancer Res. 2012;72(20):5188–97.
53. Treilleux I, Blay JY, Bendriss-Vermare N, Ray-Coquard I, Bachelot T, Guastalla JP, et al. Dendritic cell infiltration and prognosis of early stage breast cancer. Clin Cancer Res. 2004;10(22):7466–74.
54. Horton BL, Morgan DM, Momin N, Zagorulya M, Torres-Mejia E, Bhandarkar V, et al. Lack of CD8(+) T cell effector differentiation during priming mediates checkpoint blockade resistance in non-small cell lung cancer. Sci Immunol. 2021;6(64):eabi8800.
55. Wolf D, Sopper S, Pircher A, Gastl G, Wolf AM. Treg(s) in Cancer: Friends or Foe? J Cell Physiol. 2015;230(11):2598–605.
56. Budimir N, Thomas GD, Dolina JS, Salek-Ardakani S. Reversing T-cell Exhaustion in Cancer: Lessons Learned from PD-1/PD-L1 Immune Checkpoint Blockade. Cancer Immunol Res. 2022;10(2):146–53.
57. Liu C, Liu X, Xiang X, Pang X, Chen S, Zhang Y, et al. A nanovaccine for antigen self-presentation and immunosuppression reversal as a personalized cancer immunotherapy strategy. Nature Nanotechnology. 2022;17(5):531–540.
58. Liu Y, Zhou N, Zhou L, Wang J, Zhou Y, Zhang T, et al. IL-2 regulates tumor-reactive CD8+ T cell exhaustion by activating the aryl hydrocarbon receptor. Nature Immunology. 2021;22(3):358–69.
59. Sharonov GV, Serebrovskaya EO, Yuzhakova DV, Britanova OV, Chudakov DM. B cells, plasma cells and antibody repertoires in the tumour microenvironment. Nat Rev Immunol. 2020;20(5):294–307.
60. Schwartz M, Zhang Y, Rosenblatt JD. B cell regulation of the anti-tumor response and role in carcinogenesis. J Immunother Cancer. 2016;4:40.
61. Sarvaria A, Madrigal JA, Saudemont A. B cell regulation in cancer and anti-tumor immunity. Cell Mol Immunol. 2017;14(8):662–74.
62. Iglesia MD, Parker JS, Hoadley KA, Serody JS, Perou CM, Vincent BG. Genomic Analysis of Immune Cell Infiltrates Across 11 Tumor Types. J Natl Cancer Inst. 2016;108(11):djw144.
63. Lohr M, Edlund K, Botling J, Hammad S, Hellwig B, Othman A, et al. The prognostic relevance of tumour-infiltrating plasma cells and immunoglobulin kappa C indicates an important role of the humoral immune response in non-small cell lung cancer. Cancer Lett. 2013;333(2):222–8.
64. Bolotin DA, Poslavsky S, Davydov AN, Frenkel FE, Fanchi L, Zolotareva OI, et al. Antigen receptor repertoire profiling from RNA-seq data. Nat Biotechnol. 2017;35(10):908–11.
65. Mohammed ZM, Going JJ, Edwards J, Elsberger B, McMillan DC. The relationship between lymphocyte subsets and clinicopathological determinants of survival in patients with primary operable invasive ductal breast cancer. Br J Cancer. 2013;109(6):1676–84.
66. Charoentong P, Finotello F, Angelova M, Mayer C, Efremova M, Rieder D, et al. Pan-cancer Immunogenomic Analyses Reveal Genotype-Immunophenotype Relationships and Predictors of Response to Checkpoint Blockade. Cell Rep. 2017;18(1):248–62.
67. Iglesia MD, Vincent BG, Parker JS, Hoadley KA, Carey LA, Perou CM, et al. Prognostic B-cell signatures using mRNA-seq in patients with subtype-specific breast and ovarian cancer. Clin Cancer Res. 2014;20(14):3818–29.
68. Gentles AJ, Newman AM, Liu CL, Bratman SV, Feng W, Kim D, et al. The prognostic landscape of genes and infiltrating immune cells across human cancers. Nat Med. 2015;21(8):938–45.
69. Wang JZ, Zhang YH, Guo XH, Zhang HY, Zhang Y. The double-edge role of B cells in mediating antitumor T-cell immunity: Pharmacological strategies for cancer immunotherapy. Int Immunopharmacol. 2016;36:73–85.
70. Shalapour S, Font-Burgada J, Di Caro G, Zhong Z, Sanchez-Lopez E, Dhar D, et al. Immunosuppressive plasma cells impede T-cell-dependent immunogenic chemotherapy. Nature. 2015;521(7550):94–8.
71. Zhang Y, Morgan R, Podack ER, Rosenblatt J. B cell regulation of anti-tumor immune response. Immunol Res. 2013;57(1-3):115–24.
72. Zheng M, Xing C, Xiao H, Ma N, Wang X, Han G, et al. Interaction of CD5 and CD72 is involved in regulatory T and B cell homeostasis. Immunol Invest. 2014;43(7):705–16.

73. Jardim DL, Goodman A, de Melo Gagliato D, Kurzrock R. The Challenges of Tumor Mutational Burden as an Immunotherapy Biomarker. Cancer Cell. 2021;39(2):154–73.

SUPPORTING INFORMATION

Additional supporting information can be found online in the Supporting Information section at the end of this article.

How to cite this article: Ding S, Qiao N, Zhu Q, Tong Y, Wang S, Chen X, et al. Single-cell atlas reveals a distinct immune profile fostered by T cell-B cell crosstalk in triple negative breast cancer. 2023;1–24.
https://doi.org/10.1002/cac2.12429